NeuroImage 255 (2022) 119208

Contents lists available at ScienceDirect

NeuroImage

journal homepage: www.elsevier.com/locate/neuroimage

Resting-state BOLD functional connectivity depends on the heterogeneity of capillary transit times in the human brain A combined lesion and simulation study about the influence of blood flow response timing

Sebastian C. Schneider[a,b,d,1], Mario E. Archila-Meléndez[a,b,1], Jens Göttler[a,b], Stephan Kaczmarz[a,b,c], Benedikt Zott[a,b], Josef Priller[d], Michael Kallmayer[e], Claus Zimmer[a], Christian Sorg[a,b,d], Christine Preibisch[a,b,f,*]

[a] Department of Diagnostic and Interventional Neuroradiology, Technical University of Munich, School of Medicine, Klinikum rechts der Isar, Ismaningerstr. 22, 81675 Munich, Germany
[b] TUM Neuroimaging Center, Technical University of Munich, School of Medicine, Klinikum rechts der Isar, Ismaningerstr. 22, 81675 Munich, Germany
[c] Philips GmbH Market DACH, Hamburg, Germany
[d] Department of Psychiatry, Technical University of Munich, School of Medicine, Klinikum rechts der Isar, Ismaningerstr. 22, 81675 Munich, Germany
[e] Department of Vascular and Endovascular Surgery, Technical University of Munich, School of Medicine, Klinikum rechts der Isar, Ismaningerstr. 22, 81675 Munich, Germany
[f] Department of Neurology, Technical University of Munich, School of Medicine, Klinikum rechts der Isar, Ismaningerstr. 22, 81675 Munich, Germany

ARTICLE INFO

Keywords:
BOLD signal fluctuations
Resting state fMRI
BOLD-based functional connectivity
Neurovascular coupling
Capillary transit-time heterogeneity
Dynamic BOLD modeling

ABSTRACT

Functional connectivity (FC) derived from blood oxygenation level dependent (BOLD) functional magnetic resonance imaging at rest (rs-fMRI), is commonly interpreted as indicator of neuronal connectivity. In a number of brain disorders, however, metabolic, vascular, and hemodynamic impairments can be expected to alter BOLD-FC independently from neuronal activity. By means of a neurovascular coupling (NVC) model of BOLD-FC, we recently demonstrated that aberrant timing of cerebral blood flow (CBF) responses may influence BOLD-FC. In the current work, we support and extend this finding by empirically linking BOLD-FC with capillary transit time heterogeneity (CTH), which we consider as an indicator of delayed and broadened CBF responses. We assessed 28 asymptomatic patients with unilateral high-grade internal carotid artery stenosis (ICAS) as a hemodynamic lesion model with largely preserved neurocognitive functioning and 27 age-matched healthy controls. For each participant, we obtained rs-fMRI, arterial spin labeling, and dynamic susceptibility contrast MRI to study the dependence of left-right homotopic BOLD-FC on local perfusion parameters. Additionally, we investigated the dependency of BOLD-FC on CBF response timing by detailed simulations. Homotopic BOLD-FC was negatively associated with increasing CTH differences between homotopic brain areas. This relation was more pronounced in asymptomatic ICAS patients even after controlling for baseline CBF and relative cerebral blood volume influences. These findings match simulation results that predict an influence of delayed and broadened CBF responses on BOLD-FC. Results demonstrate that increasing CTH differences between homotopic brain areas lead to BOLD-FC reductions. Simulations suggest that CTH increases correspond to broadened and delayed CBF responses to fluctuations in ongoing neuronal activity.

Abbreviations: ICAS, internal carotid artery stenosis; MRI, magnetic resonance imaging; fMRI, functional magnetic resonance imaging; rs-fMRI, resting state fMRI; BOLD, blood oxygenation level dependent; BOLD-FC, rs-fMRI-based measure of functional connectivity; BOLD-TC, BOLD signal time curve; δS_{BOLD}, percentage peak-to-peak BOLD amplitude; DSC, dynamic susceptibility contrast; CTH, capillary transit time heterogeneity; CBV, cerebral blood volume; rCBV, relative cerebral blood volume; ASL, arterial spin labeling; pCASL, pseudo-continuous ASL; CBF, cerebral blood flow; CVR, cerebrovascular reactivity; $CMRO_2$, cerebral metabolic rate of oxygen; LMM, linear-mixed model.

* Corresponding author at: Department of Diagnostic and Interventional Neuroradiology, Technical University of Munich, School of Medicine, Klinikum rechts der Isar, Ismaningerstr. 22, 81675 Munich, Germany
E-mail address: preibisch@tum.de (C. Preibisch).

[1] These authors contributed equally to this study

https://doi.org/10.1016/j.neuroimage.2022.119208.
Received 4 November 2021; Received in revised form 23 February 2022; Accepted 11 April 2022
Available online 12 April 2022.

1. Introduction

Blood oxygenation level dependent (BOLD) functional magnetic resonance imaging (fMRI) signals are commonly acquired in the resting-state (rs-fMRI), in order to characterize human ongoing neuronal activity. Among BOLD-derived measures, the investigation of correlated infra-slowly fluctuating BOLD signals between brain areas (i.e., BOLD functional connectivity, BOLD-FC) stands out, as they enable brain-wide coherence analysis of organized ongoing activity and underpinning neuronal connectivity (Buckner et al., 2013; Fox and Raichle, 2007). Accordingly, BOLD-FC is widely used not only to characterize typical functional connectivity networks of the human brain (Allen et al., 2011; Yeo et al., 2011) but also impaired network organization in patients with brain disorders (Gratton et al., 2020). Critically, the common interpretation of BOLD-FC assumes that neurovascular coupling (NVC), i.e., the relationship between neuronal activity, mediating metabolic and vascular processes, and investigated BOLD signal fluctuations, is fixed across subjects, brain regions and cortical depths. In brain disorders, however, metabolic, vascular, and hemodynamic processes may distinctively alter NVC processes beyond potential alterations in neuronal activity, and thereby impact on both BOLD signal time courses (BOLD-TCs) and derived measures including BOLD-FC. For example, pronounced alterations in oxygen metabolism, vascular properties, and perfusion have been observed in brain vascular, neurodegenerative, and neuropsychiatric disorders such as stroke, Alzheimer's disease and schizophrenia, and even healthy aging (Ances et al., 2009; De Vis et al., 2015; Gottler et al., 2019a; Gottler et al., 2020; Gottler et al., 2019b; Kaczmarz et al., 2021; Kaczmarz et al., 2018; Katsel et al., 2017; Preibisch et al., 2011; Richter et al., 2017; Riederer et al., 2018; Tsvetanov et al., 2016; West et al., 2019). Notably, the impact of NVC changes on BOLD-FC is mostly ignored (Tsvetanov et al., 2021), mainly due to limited understanding of the complex non-linear influences of NVC processes on BOLD-FC.

To address this problem of limited understanding of distinctive influences of NVC processes on BOLD-FC, we recently developed a dynamic resting-state BOLD-FC simulation model, based on empirically supported biophysical NVC mechanisms (Archila-Melendez et al., 2020). We applied this model in order to simulate the effects of both impaired amplitudes and delays of metabolic and vascular-hemodynamic responses to fluctuations in neuronal activity. While we observed simple linear effects of response amplitude impairments for both cerebral blood flow (CBF) and cerebral metabolic rate of oxygen ($CMRO_2$) on BOLD-FC, effects of CBF and $CMRO_2$ *response timing* (i.e., response delays and broadening) were complex and non-linear. These theoretical results are broadly supported by findings of prominent influence of reduced perfusion, impaired cerebrovascular reactivity (CVR), and altered hemodynamic response function on BOLD-fMRI in various brain disorders and even healthy aging (D'Esposito et al., 2003; Gottler et al., 2019b; Lewis et al., 2020; Mark et al., 2015; Tsvetanov et al., 2016; van Niftrik et al., 2019; West et al., 2019). However, with respect to the influence of perfusion timing on BOLD signals, most existing studies do not focus on local perfusion but rather consider systemic delays (Christen et al., 2015; Lv et al., 2013; Siegel et al., 2016; Tong et al., 2017; Tong et al., 2019). Instead, the focus of the current study is on local NVC effects of perfusion timing on BOLD-FC, which, at least to our knowledge, has not been directly investigated in humans yet.

With respect to local CBF response timing, so-called capillary transit time heterogeneity (CTH) is a promising parameter (Jespersen and Ostergaard, 2012). CTH refers to the distribution of red blood cell capillary transit times that can be directly observed in animals. Interestingly, neural activation does not only increase blood flow but also leads to more homogeneous flow patterns of red blood cells, i.e., decreases in CTH (Jespersen and Ostergaard, 2012; Kleinfeld et al., 1998; Schulte et al., 2003; Stefanovic et al., 2008). Critically, CTH is also accessible in humans by parametric modeling of dynamic susceptibility contrast (DSC) MRI data (Mouridsen et al., 2014). While CTH impairments have been suggested to play a role and also been demonstrated in neurodegenerative and symptomatic vascular brain diseases (Mundiyanapurath et al., 2016; Nielsen et al., 2020; Ostergaard et al., 2013a; Ostergaard et al., 2016; Ostergaard et al., 2013b; Potreck et al., 2019), we recently demonstrated ipsilateral CTH increases in asymptomatic patients with unilateral internal carotid artery stenosis (ICAS) (Kaczmarz et al., 2021). These patients show clear vascular-hemodynamic deficits, i.e., ipsilateral reductions in CBF and CVR along with significantly increased CBV, which are particularly pronounced in individual watershed areas. However, compared to healthy controls oxygen extraction fraction (OEF) and $CMRO_2$ are preserved (Kaczmarz et al., 2021; Gottler et al., 2019a), with $CMRO_2$ being elevated contralateral to the stenosis (Gottler et al., 2019a). In line with largely unchanged oxygen metabolism that is commonly considered as a proxy of neuronal activity, these patients' neurocognitive functioning is largely preserved except for subtle deficits in visual attention (Gottler et al., 2020). Thus, asymptomatic unilateral ICAS provides an interesting lesion model of one-sided impaired vascular-hemodynamics at largely preserved neuronal functioning, which allows to study the influence of local perfusion variability – in particular CTH – on BOLD-FC between homotopic left-right hemisphere region pairs.

In the current study, we primarily hypothesized that changes in CTH impact BOLD-FC. To test this hypothesis empirically, we studied the relation between left-right pairwise homotopic BOLD-FC and local CTH in patients with asymptomatic unilateral ICAS and healthy controls, while controlling for baseline CBF and relative cerebral blood volume (rCBV). Secondarily, we hypothesized that CTH might serve as an indicator for timing aspects of the local microvascular CBF response. With respect to this second hypothesis, we first analyzed CBF timing impact on BOLD-FC via a simulation approach using our recently established NVC model (Archila-Melendez et al., 2020). Then we compared and discussed in detail effects of both CTH and CBF response timing on BOLD-FC. The latter investigation should be understood as a preliminary first step towards a more in-depth analysis of the general physiological link between timing aspects of NVC and BOLD-FC.

2. Materials and methods

Our study has three parts. First, we performed an empirical study in patients with asymptomatic ICAS and healthy controls regarding the impact of CTH on BOLD-FC (see methods Section 2.1.). Second, we studied – in a simulation study – the impact of CBF response timing on BOLD-FC (see methods Section 2.3.). The third part of our study regards a potential link between CTH and CBF response timing and their effects on BOLD-FC (see methods Section 2.2.) that is further scrutinized in the second half of the discussion.

2.1. Empirical study: CTH and BOLD-FC

We analyzed multi-parametric hemodynamic MRI data, namely BOLD-fMRI, arterial spin labeling (ASL) and dynamic susceptibility contrast (DSC) MRI, from asymptomatic ICAS patients and age-matched healthy controls. From our subject cohort, analyses regarding hemodynamic impairments in ICAS have been published previously (Gottler et al., 2019a; Gottler et al., 2020; Kaczmarz et al., 2021; Kaczmarz et al., 2018). Here, we derived BOLD-FC from BOLD-fMRI data and investigated its relation to hemodynamic alterations, in particular changes in CTH.

2.1.1. Participants

From an existing sample of 29 ICAS patients and 30 age-matched controls, which we analyzed previously (Gottler et al., 2019a; Gottler et al., 2020; Kaczmarz et al., 2021; Kaczmarz et al., 2018), we included data from 28 ICAS patients (11 females) and 27 healthy controls (15 females), from whom all necessary data are available and of sufficient quality, leading to an overall sample size of 55 participants.

Table 1
Summary of participant characteristics.

	ICAS (N=28)	Control (N=27)	*p*
Age (years)			0.99
- mean (SD)	70.1 (7.1)	70.1 (4.9)	
- range	52.0 - 84.0	61.0 - 77.0	
Sex			0.23
- female: N (%)	11 (39.3)	15 (55.6)	
- male: N (%)	17 (60.7)	12 (44.4)	
Side of Stenosis			
- left N (%)	11 (39.3)	0	
- right N (%)	17 (60.7)	0	
Stenotic degree (% NASCET): mean (SD)	80.9 (9.6)	-	
Handedness - right: N (%)	25 (89.3)	26 (96.3)	0.63
BMI: mean (SD)	26.3 (4.9)	27.1 (4.2)	0.52
Smoking [packs per year] : mean (SD)	15.3 (22.1)	8.4 (14.4)	0.17
Fazekas: mean (SD)	1.5 (0.8)	0.9 (0.9)	**0.02**
PAOD: N (%)	8 (28.6)	3 (11.1)	0.11
CHD: N (%)	9 (33.3%)	2 (7.4%)	**0.02**
Hypertension: N (%)	22 (78.6)	15 (55.6)	0.07
BP [mmHG]			
- systolic: mean (SD)	154.2 (25.0)	141.7 (18.7)	**0.04**
- diastolic: mean (SD)	85.7 (10.1)	85.1(6.9)	0.80
Diabetes: N (%)	7 (25.9)	2 (7.4)	0.07
Statins: N (%)	20 (71.4)	5 (18.5)	**< 0.001**
Antiplatelets: N (%)	25 (89.3)	5 (18.5)	**< 0.001**
Antihypertensives: N (%)	19 (67.9)	11 (40.7)	0.25
Antidiabetics: N (%)	4 (14.3)	2 (7.4)	0.25
MMSE: mean (SD)	28.2 (2.4)	28.7 (1.4)	0.39
TMT-A: mean (SD)	49.7 (23.4)	41.8 (13.2)	0.13
TMT-B: mean (SD)	139.5 (63.7)	103.2 (39.3)	**0.02**
LBT [abs. % deviation from center] : mean (SD)	2.3 (2.1)	3.1 (1.8)	0.16
BDI: mean (SD)	9.9 (9.8)	8.4 (5.2)	0.51
STAI: mean (SD)	38.6 (10.7)	34.9 (10.1)	0.22

Note: Variables are represented by either mean and standard deviation (SD) or absolute number N and fraction in percent. Two-sample t-tests were used for group comparisons in age, mean pack-years, BP, BMI, MMSE, TMT-A/B, BDI, STAI, and LBT; Chi-squared test for remaining group comparisons. Bold print indicates significant group differences $p < 0.05$. Abbreviations: BMI, body mass index; PAOD, peripheral artery occlusive disease; CHD, coronary heart disease; BP, blood pressure; MMSE, mini mental state exam; TMT-A/B, trail making test-A/B; LBT, line bisection test; BDI, Beck's depression inventory; STAI, state trait anxiety inventory.

Median age of participants from both groups was 71 years (age range: 52–84 years; mean age: 70.1 years; no significant group differences). The asymptomatic ICAS patients had an unilateral, high-grade stenosis of the extracranial internal carotid artery (11 with left-sided stenosis; each stenosis was > 70% as defined by NASCET (1991)). All participants underwent extensive medical testing to exclude neurological, psychiatric and chronic kidney diseases, which constituted exclusion criteria along with incidental MRI findings hinting at brain lesions (e.g. stroke). The study was approved by the medical ethical board of the Klinikum rechts der Isar; for a detailed description of the overall sample characteristics see Table 1. Participants provided written informed consent to all conducted examinations.

2.1.2. MRI acquisition, BOLD signal preprocessing and calculation of hemodynamic parameter maps

Next, we describe our MRI protocol and signal processing procedures resulting in our outcome measures of BOLD-FC, CTH, CBF and rCBV.

MRI acquisition: All MR imaging was conducted using a 3T Philips Ingenia MR-Scanner (Philips Healthcare, Best, The Netherlands) and a 32-channel head coil. Brain parcellation and lesion detection was derived from anatomical MRI data, namely T_1-weighted magnetization prepared rapid gradient echo (MPRAGE; TE = 4 ms, TR = 9 ms, $\alpha = 8^\circ$, TI = 1000 ms, shot interval = 2300 ms, SENSE AP/RL 1.5/2.0, 170 slices, matrix size = 240 × 238, voxel size = 1 × 1 × 1 mm^3) and T2-weighted fluid attenuated inversion recovery (FLAIR; TE = 289 ms, TR = 4800 ms, inversion delay = 1650 ms, TSE factor = 167, 163 slices, matrix size = 224 × 224, voxel size = 1.12 mm^3 isotropic). BOLD-TCs and BOLD-FC were derived from T_2*-weighted multiband echo planar imaging (EPI) time series (TE = 30 ms, TR = 1.2 s, $\alpha = 70^\circ$, multiband factor 2, SENSE factor 2, 38 slices, matrix size = 192 × 192, voxel size = 3 × 3 × 3 mm^3, 500 dynamic scans, scan duration 10 min). CTH and rCBV were derived from DSC MRI (80 single-shot EPI volumes, TE = 30 ms, TR = 1513 ms, $\alpha = 60^\circ$, 26 slices, voxel size = 2.0 × 2.0 × 3.5 mm^3, bolus injection of Gd-Dota (concentration 0.5 mmol/ml, dose 0.1 mmol/kg, at least 7.5 mmol per subject)). Lastly, baseline CBF was derived from pseudo-continuous arterial spin labeling (pCASL) acquisitions (post label delay (PLD) = 2000 ms, label duration = 1800 ms, 16 slices). To maximize the number of eligible subjects as well as data quality, we included for each subject the highest quality CBF map from pCASL data that were acquired for sequence comparisons (Kaczmarz et al., 2016). For the majority of 40 subjects, a 3D gradient spin echo (GRASE) readout with 4 background suppression (BGS) pulses, TE/TR/α = 7.4 ms/ 4377 ms/90°, turbo spin echo factor 19, EPI factor 7, voxel size = 2.75 × 2.75 × 6 mm^3 was employed. For the remaining subjects, sequences with a 2D EPI readout and similar acquisition parameters were used, with either 4 BGS pulses (6 subjects), 2 BGS pulses (7 subjects), or no BGS (2 subjects).

BOLD signal preprocessing: Preprocessing of BOLD fMRI and anatomical MRI data was done with the Data Processing Assistant for Resting-State fMRI advanced edition (DPARSFA) toolbox V5.0_200401 (Chao-Gan and Yu-Feng, 2010) and SPM12 (v7771; Wellcome Trust Centre for Neuroimaging, UCL, London, UK) using MATLAB (R2019b; MathWorks, Natick, MA, USA). This minimal preprocessing approach included realignment of the EPI time series data, manual reorientation of all images along the anterior–posterior commissure (AC–PC), cropping of the anatomical data, spatial co-registration of anatomical and fMRI data, brain extraction and Diffeomorphic Anatomical Registration Through Exponentiated Lie Algebra (DARTEL) segmentation of the anatomical images, nuisance covariate regression including six motion parameters and a linear trend regressor, smoothing with a 6 mm Full Width at Half

Maximum (FWHM) Gaussian kernel and applying a temporal bandpass filter from 0.01 to 0.1 Hz.

NVC parameter map calculation: CTH, rCBV and CBF parameter maps were calculated with custom MATLAB programs (R2016b; MathWorks, Natick, MA, USA). Spatial coregistration and segmentation were performed with SPM12 (Wellcome Trust Centre for Neuroimaging, UCL, London, UK) as previously described in detail (Kaczmarz et al., 2021).

Preprocessing of DSC data comprised correction for motion and slice timing effects. CTH and rCBV parameter maps were then derived from relative concentration time curves that were calculated from the time course signal $S(t)$ according to $C(t) \propto \Delta R_2(t) = -\ln(\frac{S(t)}{S(0)})/TE$ (Østergaard et al., 1999).

Calculation of CTH parameter maps employed parametric modeling of $C(t)$ (Jespersen and Ostergaard, 2012; Mouridsen et al., 2014). To achieve model-based estimation of the tissue residue function $R(t)$, a gamma variate function with parameters α and β is employed to parametrize the probability density distribution $h(\tau)$ of capillary transit times τ (across a capillary bed of parallel capillaries)

$$h(\tau;\ \alpha, \beta) = -\frac{dR}{d\tau} = -\frac{1}{\beta^{\alpha}\Gamma(\alpha)}\tau^{\alpha-1}e^{-\tau/\beta}. \quad (1)$$

Parameter estimation is then performed by an expectation–maximization-type algorithm, which permits inclusion of prior information (Mouridsen et al., 2006). Using the parametrization according to Eq. (1), CTH is determined as the standard deviation of the capillary transit time distribution ($\sigma = \sqrt{\alpha}\beta$) in seconds, with larger values indicating a larger heterogeneity. The vascular mean transit time (MTT) can be obtained as $\mu = \alpha\beta$.

For CBV calculation, leakage correction of the concentration time curve $C(t)$ was performed as described previously (Kluge et al., 2016). Relative CBV was then calculated by integrating the leakage corrected concentration time curve (Hedderich et al., 2019; Kluge et al., 2016). Resulting rCBV maps were re-referenced to normal appearing white matter (NAWM) with CBV=2.5% (Leenders, 1994).

Quantitative baseline CBF maps were derived from the pCASL data following recommendations outlined in the ISMRM perfusion study group consensus paper (Alsop et al., 2015). In short, the label and control images were motion corrected separately, differences averaged after pairwise subtraction, and CBF calculated according to Eq. (1) from (Alsop et al., 2015) with M_0 being used for normalization. The resulting CBF maps were smoothed using a 5 mm isotropic Gaussian kernel.

2.1.3. BOLD-FC, CTH, baseline CBF, and rCBV in homotopic left-right region pairs

For our analysis, we focused on pairwise homotopic BOLD-FC, as correlated BOLD signal fluctuations between homotopic left-right volumes-of-interest (VOIs) are unlikely to be affected by incoherent vascular geometry, blood arrival times, vasomotion, and neural activity (Drew et al., 2020). Those factors have been shown to be largely comparable due to both the brain's symmetrical anatomy and cross-hemispheric fiber connectivity (see (Drew et al., 2020) for a comprehensive review). Furthermore, functional connectivity between homotopic VOIs provides relatively strongest BOLD-FC values compared to within-hemisphere or non-homotopic across hemisphere VOI pairs, likely due to supporting pairwise homotopic structural connectivity (Drew et al., 2020). Thus, homotopic pairwise BOLD-FC is an excellent paradigm for analyzing the impact of one-sided NVC alterations on BOLD-FC.

VOI Selection: To obtain left-right pairwise homotopic BOLD-FC, we used the Atlas of Intrinsic Connectivity of Homotopic Areas (AICHA) (Joliot et al., 2015). The AICHA was derived from resting-state BOLD-FC of a large sample of healthy participants (N = 281), with the parcellation algorithm being explicitly weighted towards the homotopic organization of the brain and its functional separation, resulting in an atlas being ideally suited for BOLD fMRI analyses of homotopic areas. It provides overall 384 anatomically labeled VOIs, which can be separated in 192 cross-hemispheric VOI pairs, covering cortical and subcortical grey matter areas of the forebrain.

BOLD-FC Analysis: All analyses involving pairwise BOLD-FC and NVC parameter maps were performed in the individual participants' native space. To this end, we adapted the AICHA to each individual's native anatomy via a non-linear transformation using the reverse flow fields that we obtained by MNI normalization of the individual anatomical MRI data (T1-weighted MPRAGE). The AICHA atlas was then resliced to match the resolution of the functional MRI data used in our study. To ensure maximum overlap with the individual participants' brain anatomy, the atlas was masked with a grey matter (GM) mask derived from the individual participants' segmented MPRAGE data ($p_{GM} > 0.3$, resliced to fMRI resolution). To this end, individual GM probability maps were obtained by segmenting each subject's MPRAGE data with SPM12 (Wellcome Trust Centre for Neuroimaging, UCL, London, UK) using default settings. For each participant, VOI-average BOLD-TCs were then extracted from all 384 VOIs and correlated using Pearson's correlation between the left and right homotopic areas. Correlation coefficients were then Fisher-r-to-z transformed to obtain 192 pairwise BOLD-FC values for each participant.

NVC Parameter Analysis: Similarly, differences in CTH, baseline CBF and rCBV parameter values were extracted from these homotopic VOI pairs. The AICHA atlas, already in subject-space, was resliced to the respective parameter maps and subsequently masked by an accordingly resliced GM mask. For each VOI, the underlying metric was then extracted, and the differences in parameter values calculated between pairwise homotopic VOIs by subtracting the right from the left sided VOI value. In particular, ΔCTH [sec] = $CTH_{VOI\text{-}Left} - CTH_{VOI\text{-}Right}$, ΔCBF [ml/100 g/min] = $CBF_{VOI\text{-}Left} - CBF_{VOI\text{-}Right}$, and ΔrCBV [pp (percentage points)] = $rCBV_{VOI\text{-}Left} - rCBV_{VOI\text{-}Right}$. A difference of '0' means that the two homotopic areas exhibit no difference in the respective parameter values. Differences with negative or positive values reflect higher right-sided or higher left-sided parameter values, respectively, indicating an imbalance between right and left homotopic cortical areas.

As both rs-fMRI and hemodynamic MRI parameter maps did not cover the whole brain, some VOIs included either no or only very few voxels, which was enhanced by GM masking. We therefore excluded all VOIs with fewer than 10 voxels in the fMRI resolution (3×3×3 mm^3). The VOI-extracted NVC parameter differences were consequently z-standardized across all VOIs and subjects. After exclusion of VOIs based on voxel number, some VOI-average CTH, baseline CBF and rCBV parameters values still constituted outliers, i.e., implausible physiological values (e.g., due to imaging artifacts or partial volume effects with CSF). We, therefore, also excluded VOI pair differences with z-values below −2.56 and above 2.56, respectively, (i.e., 1% of extreme differences, including 99% of observations) for each parameter to remove excessive physiologically implausible differences. In total, 1844 observations were excluded (1325 due to low voxel counts, 519 due to z-score outliers), retaining 8716 observations.

2.1.4. Statistical testing of empirical BOLD-FC analyses

Group differences in BOLD-FC & NVC parameters: To test for significant group differences in pairwise BOLD-FC and NVC parameters, we computed the mean BOLD-FC as well as the mean absolute CTH, baseline CBF and rCBV differences, i.e., |ΔCTH|, |ΔCBF|, and |ΔrCBV|, for each participant across all VOI pairs. These mean values were then compared between groups using Welch's t-test. One-sample t-tests were used to test for each group separately if mean pairwise NVC parameter differences were significantly different from zero. In order to explore potential regional effects, we examined how BOLD-FC, |ΔCTH|, |ΔCBF| and |ΔrCBV| differed between the groups across 54 VOI pairs that were derived from the AICHA (Joliot et al., 2015) by merging subregions of cortical and subcortical areas, e.g., in the Thalamus, where the regions N_Thalamus-1,-2,-3 were merged to N_Thalamus, for each participant. Merging was performed to simplify the analysis by reducing the number of VOIs. In addition, we examined if the ICAS patients' mean BOLD-FC,

|ΔCTH|, |ΔCBF| and |ΔrCBV| depend on the degree of stenosis by means of a correlation analysis.

Influence of NVC parameters on BOLD-FC: To examine the influence of NVC parameters, especially of CTH, on BOLD-FC between homotopic brain regions, we regressed the influence of z-standardized pairwise NVC differences, i.e., |ΔCTH|, |ΔCBF|, and |ΔrCBV|, on pairwise BOLD-FC. We did so by means of a linear-mixed model (LMM) approach to account for the influence of multiple NVC parameters and the factor group, i.e., ICAS patients versus healthy controls, as well as to control for the participants' age and corresponding interactions, e.g., between age and influence of |ΔCTH| (see Table 3 for details). In an additional model, we further controlled for sex differences. The LMM also allowed for assessing the full complexity of a potential association by capturing the between-subject variance with regard to the group effects.

Using z-standardized regressors was necessary to enable comparison of regression effects because the effect sizes of predictors on BOLD-FC are determined by their absolute values. In our case, a difference of 1 would constitute a large difference for CTH, but only a small difference for CBF. Thus, z-standardization ensured an identical scale and range for all included parameters since a change of 1 always indicates a change of 1 standard deviation (σ) even though σ_{CTH} =2.47 s and σ_{CBF} = 5.73 ml/100g/min differed numerically.

Concretely, the LMM approach was performed by use of the lme4 package (Bates et al., 2015) for R (RCoreTeam, 2020) within Rstudio (RStudioTeam, 2019). We opted for a random-coefficient model with pairwise BOLD-FC as dependent variable and |ΔCTH|, |ΔCBF|, and |ΔrCBV| as primary regressors. Adding |ΔCBF| and |ΔrCBV| as regressors to our model allowed us to assess the specific impact of |ΔCTH| on BOLD-FC, independent of differences in baseline CBF and rCBV. In addition, we used these regressors to study the impact of CBF and rCBV on BOLD-FC, respectively. Further regressors were the participants' age and group affiliation. Age was centered on the overall median (71 years). For each of the pairwise NVC parameter differences, we further controlled for interactions with age and group affiliation. Deviations from the overall average effects among participants were controlled by including the intercepts and slopes of |ΔCTH|, |ΔCBF|, and |ΔrCBV| as random effects. The model's degrees of freedom and *p*-values were estimated via the Tests in Linear Mixed Effects Models (lmerTest) package (Kuznetsova et al., 2017) using Satterthwaite's method.

2.2. Theoretical considerations regarding the link between CTH and CBF response timing – a preliminary approximation

Beyond the impact of CTH on BOLD-FC, we were interested in a potential link between CTH and CBF response timing. Therefore, we outline some theoretical considerations about such a link and, in particular, similarities regarding the impact of CTH and CBF response timing on BOLD-FC, respectively.

To better understand the impact of timing aspects of CBF responses on BOLD-FC, we employed a recently proposed simulation framework (Archila-Melendez et al., 2020). Critically, with respect to CBF, an increase in the characteristic time constant τ_f of the gamma variate function used to model the CBF response results in an increasingly delayed and broadened CBF response function with a peak at $t = 2{\cdot}\tau_f$, a diminishing amplitude, and a constant area under the curve (for more details see Fig. 1 and Section 2.3.). Critically, this behavior resembles aspects of CTH. In particular, the distribution h of capillary transit times τ is also modelled by a gamma variate function (see Eq. (1)) to facilitate CTH measurement by parametric modeling of DSC MRI (Mouridsen et al., 2014). This similarity between CBF response function and distribution of capillary transit times $h(\tau)$ is at the core of our idea that CTH might represent critical aspects of CBF response timing, and might therefore serve as kind of an zero-order approximation. In the following, we want to clarify this similarity between CBF response and CTH in more detail.

By means of a vascular model (Jespersen and Ostergaard, 2012; Mouridsen et al., 2014), the probability density function of capillary transit times $h(\tau)$ can be parametrized by a gamma variate function with shape parameters α and β (see Eq. (1)). According to tracer kinetic theories, $h(\tau)$ corresponds to the slope of the residue function $R(t)$, which describes the washout of an intravascular tracer (Østergaard et al., 1996; Østergaard et al., 1999) and is thus related to the vascular mean transit time ($MTT = \int_{-\infty}^{\infty} \tau h(\tau) d\tau / \int_{-\infty}^{\infty} h(\tau) d\tau$) and via the central volume theorem also to CBV and CBF, i.e., MTT = CBV/CBF. Using the parametrization in Eq. (1), MTT and CTH are obtained as the mean ($\mu = \alpha\beta$) and standard deviation ($\sigma = \sqrt{\alpha}\beta$) of $h(\tau)$, respectively (Jespersen and Ostergaard, 2012). While an increase in MTT could also be accomplished by a homogenous increase in capillary transit times and could thus be used as a proxy for a merely delayed CBF response, an increase in CTH necessarily implies a broadening as well as a delay in CBF (see Eq. (6) in Østergaard et al., 1999). This correspondence in both response nature and distribution model thus supports the idea that the characteristic time constant τ_f in our simulation model resembles important aspects of measured CTH.

2.3. Simulation study: CBF response timing and BOLD-FC modeling

In order to systematically explore the dependence of BOLD-FC on CBF response timing (i.e., varying τ_f), BOLD-FC was calculated between a selected reference seed BOLD-TC (with supposedly 'healthy' parameter settings) and a range of target BOLD-TCs (with supposedly 'impaired' parameter settings). The constellation of 'healthy' and 'impaired' BOLD-TCs corresponds to the situation in our empirical analysis of pairwise homotopic BOLD-FC in ICAS patients, where BOLD-TCs from the healthy contralateral side are correlated with potentially impaired BOLD-TCs extracted from homotopic VOIs ipsilateral to the stenosis. In addition, we explicitly explored the BOLD-TCs' amplitudes and their temporal delays (lags) with respect to the selected reference seed BOLD-TC. The simulated BOLD-TCs are referred to as BOLD responses because in our simulation model they are elicited by purely sinusoidal synthetic neuronal input signals at different frequencies in the infra-slow frequency spectrum below 0.1Hz. All described calculations and simulations were implemented and performed using MATLAB (R2019b; MathWorks, Natick, MA, USA).

BOLD-TC signal model: Details of our model have been described recently (Archila-Melendez et al., 2020). Importantly, it allows for independent modeling of CBF and $CMRO_2$ responses to neuronal activity, with respect to amplitudes as well as timing characteristics. Our implementation in Simulink and MATLAB (R2019b; MathWorks, Natick, MA, USA) is similar to the one proposed by Simon and Buxton (2015), which is based on a modified balloon model (Buxton et al., 1998; Obata et al., 2004), critically extended for including extra- and intravascular BOLD signal contributions according to Obata et al. (2004). With respect to nomenclature, we stick to previous conventions and express changes in dynamic variables relative to baseline values (see Table 2).

In short, dynamic changes in normalized blood flow, $f_{in}(t)$, and oxygen consumption, $m(t)$, are modeled as linear responses to a prescribed neuronal input $N(t)$ by convolution of $N(t)$ with scaled gamma distributions $h_{f,m}(t)$, which are defined independently for flow (f) and metabolic (m) input functions, respectively (Archila-Melendez et al., 2020)

$$f_{in}(t) = N(t) * h_f(t) \tag{2}$$

$$m(t) = N(t) * h_m(t) \tag{3}$$

with

$$h_{f,m}(t) = H_{f,m} \frac{1}{\tau_{f,m}(z-1)!} \left(\frac{t}{\tau_{f,m}}\right)^{(z-1)} e^{-t/\tau_{f,m}} \tag{4}$$

The shape parameter z, scaling parameters $H_{f,m}$, and characteristic time constants $\tau_{f,m}$ take distinct values for flow (f) and metabolic (m) input functions, respectively (see Table 2). From both flow, $f_{in}(t)$, and oxygen consumption, $m(t)$, inputs, a system of coupled differential equations

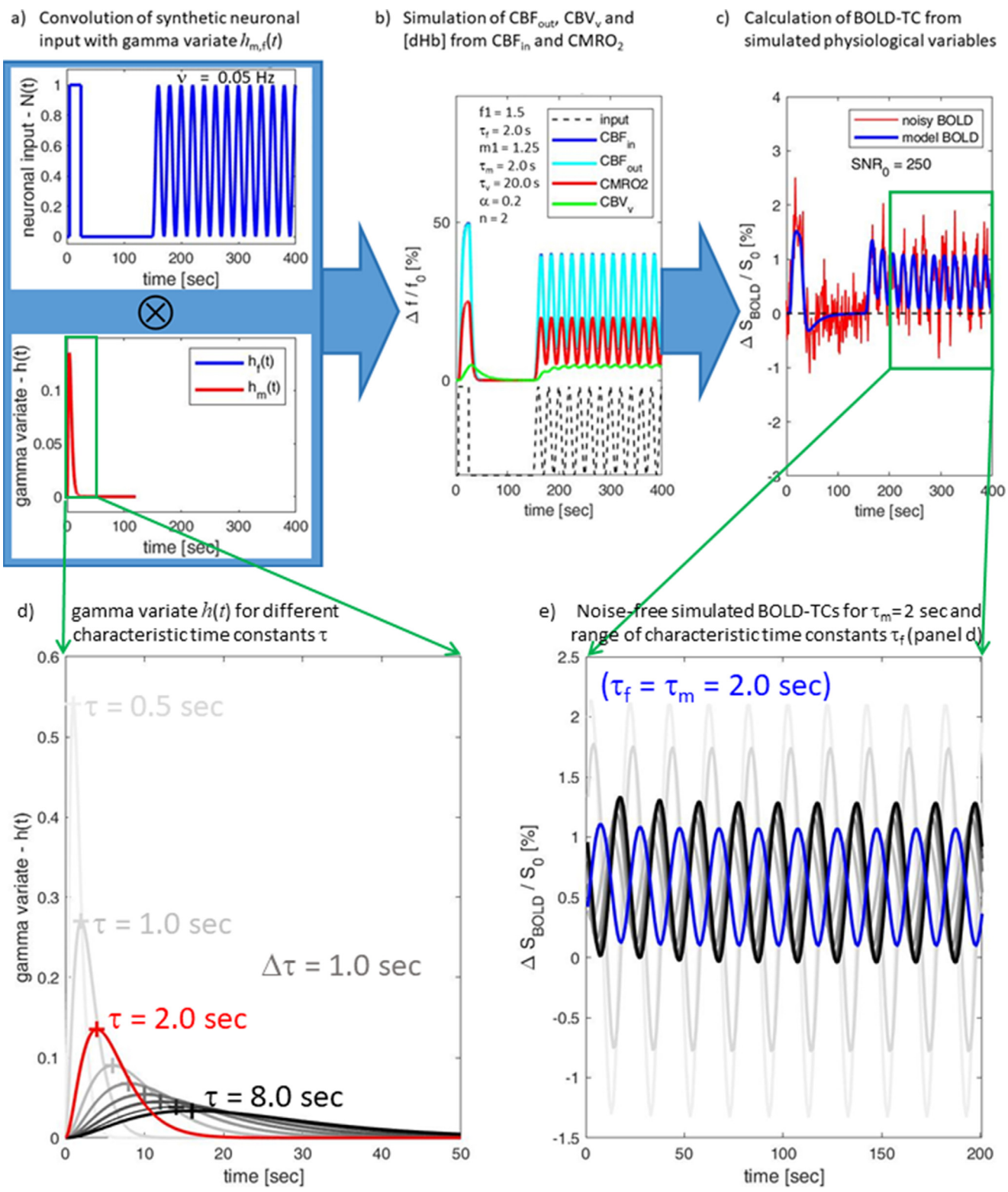

Fig. 1. Illustration of the BOLD signal time course (BOLD-TC) simulation process for the reference BOLD-TC (seed) (a-c) together with gamma variate response functions $h(t)$ (d) and BOLD-TCs for a range of characteristic time constants τ_f of blood flow response (e). (a) A purely sinusoidal input signal $N(t)$ with a frequency of 0.05 Hz is coupled to an initial boxcar portion (top) and convoluted with gamma variate functions $h_f(t)$ and $h_m(t)$ (bottom; note that both functions are overlapping). (b) This yields independent normalized inputs $f_{in}(t)$ (CBF_{in}) and $m(t)$ ($CMRO_2$), which were used to simulate blood flow out of the tissue ($CBF_{out} \approx CBF_{in}$), venous CBV ($CBV_v$) and deoxyhemoglobin content [dHb] assuming a slow CBV response (τ_v = 20.0 s). (c) The resulting BOLD-TC (blue) with a temporal resolution of TR = 1000 ms is complemented with random white noise to yield a noisy BOLD-TC (red) with SNR_0 = 250. The signal portion used for BOLD-FC calculations is marked by a green frame. (d) Gamma variate response functions $h(t)$ and (e) BOLD-TCs for a range of characteristic time constants τ_f of blood flow response. (d) The $h(t)$ with τ = 2.0 s (corresponding to the condition in panel (a)) is highlighted in red. The remaining curves range between τ = 0.5 s and [1.0, …, 8.0] s with $\Delta\tau$ = 1 s. Note that $h(t)$ peaks at $t = 2{\cdot}\tau$ and the amplitude decreases such that the area under the curve remains constant. The BOLD-TCs in panel (e) were simulated for the range of characteristic time constants τ_f (as shown in panel (d)) and τ_m = 2.0 s. Note that the colors are matched to panel (d) but the BOLD-TC with τ_f = 2.0 s (corresponding to the condition in panel (c)) is highlighted in blue.

Table 2
Summary of dynamic model parameters following (Archila-Melendez et al., 2020; Blockley et al., 2009; Buxton et al., 2004; Simon and Buxton, 2015). Default settings employed for simulation of the reference seed BOLD-TC are accentuated by bold print.

Parameter	Description	Value
$N(t)$	input intrinsic neuronal activity at time t	dynamic [0 - 1]
$m(t)$	ratio of CMRO2 to baseline at time t	Dynamic
$m1$	CMRO2 'response' amplitude	**1.25**
$f_{in}(t)$	ratio of CBF inflow to baseline at time t	dynamic
f_1	CBF 'response' amplitude	**1.5**
$f_{out}(t)$	ratio of CBF outflow at time t to baseline	dynamic
$q(t)$	ratio of deoxyhemoglobin quantity at time t to baseline	dynamic
$v(t)$	ratio of venous CBV at time t to baseline	dynamic
$h_{f,m}(t)$	convolution kernel relating CBF and CMRO2 to neuronal input	variable
$H_{f,m}$	scaling parameter for CBF and CMRO2 convolution kernels	variable
τ_m	characteristic time constants for CMRO2	**2 s**
τ_f	characteristic time constants for CBF:	
	- reference seed BOLD-TC	**2 s**
	- target BOLD-TCs	[0.5–8.0] sec
α_v	exponent describing steady state venous flow-volume coupling	**0.2**
τ_v	characteristic time constants for venous CBV response	**20 s**
ν_0	frequency offset of a fully deoxygenated blood vessel at 3 T	80.6 s^{-1}
r_0	slope defining the dependence of the $R2^*$ on blood oxygenation at 3T	178 s^{-1}
ε	intrinsic ratio of blood to tissue signals at rest at 3T	0.24
τ_0	transit time for blood through venous compartment	0.75 s
Z	shape parameter for CBF and CMRO? convolution kernels	3

is used to derive relative changes in deoxyhemoglobin content, $q(t)$, and venous blood volume, $v(t)$ (see Eqs. (6)-(10) in (Archila-Melendez et al., 2020)). Based on $q(t)$ and $v(t)$, BOLD signal changes relative to baseline are calculated accounting for extra- and intravascular signal contributions (see Eq. (5) in (Archila-Melendez et al., 2020)). The simulation process is illustrated in Fig. 1 and employed parameters and their settings as summarized in Table 2.

Fig. 1 demonstrates that the employed simulation model is capable of simulating a wide range of NVC-behaviors that have been observed in empirical studies. On the one hand, the initial block stimulus (Fig. 1a, top, left) causes a strong and prolonged CBV response that causes a distinct BOLD signal undershoot (Fig. 1c, left), on the other hand, the infra-slow oscillatory neuronal input (Fig. 1a, top, right) induces hardly recognizable CBV oscillations in the steady state (Fig. 1b, right) but distinct BOLD signal oscillations (Fig. 1c, right – green framed portion between 200 and 400 sec; see (Archila-Melendez et al., 2020) for a detailed discussion). Fig. 1d illustrates the behavior of $h_f(t)$: With increasing characteristic time constant τ_f, the peak is not only delayed but the curve broadens and the amplitude is reduced in a way that the area under the curve remains constant. Fig. 1e finally shows BOLD-TCs that were simulated with different τ_f (as shown in Fig. 1d) at $\tau_m = 2.0$ s. It can clearly be seen that a change in τ_f influences amplitude as well as phase of the resulting BOLD-TC signals presented in Fig. 1e.

Matrix representation of BOLD-TCs in the (τ_f, ν) parameter space: BOLD-TCs were simulated across a 16 × 10 matrix, where the characteristic time constant τ_f of the CBF response was systematically varied in 16 steps ($\Delta\tau = 0.5$ s) with $\tau_f = [0.5,\ldots, 8.0]$ sec for a range of ten purely sinusoidal input functions $N(t)$ with frequencies ν between 0.01 Hz and 0.1 Hz ($\Delta\nu = 0.01$ Hz). The same input parameters and settings were used as described in (Archila-Melendez et al., 2020) for 'Scenario 2 – $CMRO_2$ and CBF delays' at slower CBV response (see Table 2). The neuronal input functions $N(t)$ were coupled to a boxcar portion similar to previous work (Archila-Melendez et al., 2020). This allows direct comparisons between outputs of the BOLD signal model for an ultra-slow (boxcar) stimulus and the oscillatory inputs at different frequencies that are separated by a low-level constant baseline.

Matrix representations of BOLD-TC amplitudes and lags: Next, matrices of BOLD-TCs across the (τ_f, ν) parameter space were analyzed with respect to both BOLD signal peak-to-peak amplitudes δS_{BOLD} and temporal shifts (i.e., lags) of the simulated BOLD-TCs with respect to the reference seed BOLD-TCs with $\tau_f = 2.0$ s at each of ten purely sinusoidal input functions $N(t)$. This information helps to understand the CBF timing effects on BOLD-FC. Concerning BOLD-TC amplitude, δS_{BOLD} was calculated as the percentage difference between the maximum and minimum signal in the purely oscillatory 'resting' fMRI portions of the simulated BOLD-TCs (last 200 s). Concerning BOLD-TC lags, temporal shifts of the simulated BOLD signal with respect to the reference seed BOLD-TC ($\tau_m = \tau_f = 2.0$ s) were obtained by cross-correlation (Matlab function 'xcorr') from noise-free simulated BOLD-TCs, normalized by the period length of the input oscillatory signal ($T_p = [100, \ldots., 10]$ s) and reduced to a unique range of [−0.5, …., 0.5].

Matrix representations of BOLD-FC: Finally, based on the matrix representation of BOLD-TCs across the (τ_f, ν) parameter space, we studied the dependence of BOLD-FC on the characteristic time constant τ_f of the CBF response as well as on the frequency of the sinusoidal neuronal input signals $N(t)$. To this end, we performed Pearson's correlations between the reference seed BOLD-TC ($\tau_f = 2.0$ s) and the range of target BOLD-TCs ($\tau_f = [0.5,\ldots, 8.0]$ s) at each of the 10 input frequencies $\nu = [0.01, \ldots, 0.1]$ Hz. The seed and target BOLD-TCs were complemented with random white noise to achieve a signal to noise ratio (SNR) of 250. For each pair of investigated parameter values, correlations were performed for BOLD-TCs complemented by 16×16 different random white-noise realizations. For display, matrices of Pearson's correlation coefficients were Fisher-r-to-z transformed to z-values. In this work, we did not consider the influence of different noise levels and sampling frequency (i.e., repetition times) because decreasing SNR and temporal resolution have been shown to simply deteriorate the simulated BOLD-FC overall (Archila-Melendez et al., 2020).

This matrix of pairwise BOLD-FC between 'healthy' and 'impaired' regions provides us with predictions of altered BOLD-FC as a function of altered local CBF response timing at different neuronal input frequencies ν. These predictions were applied to interpret how pairwise homotopic BOLD-FC of asymptomatic patients with unilateral carotid artery stenosis and healthy controls depends on the heterogeneity of local capillary transit times, which we assume to reflect local CBF response variability in terms of response timing.

3. Results

3.1. Empirical results regarding the dependence of homotopic pairwise BOLD-FC on CTH

Distribution of BOLD-FC and NVC parameter values and their group differences: AICHA VOIs and NVC parameter maps are shown in Fig. 2a-

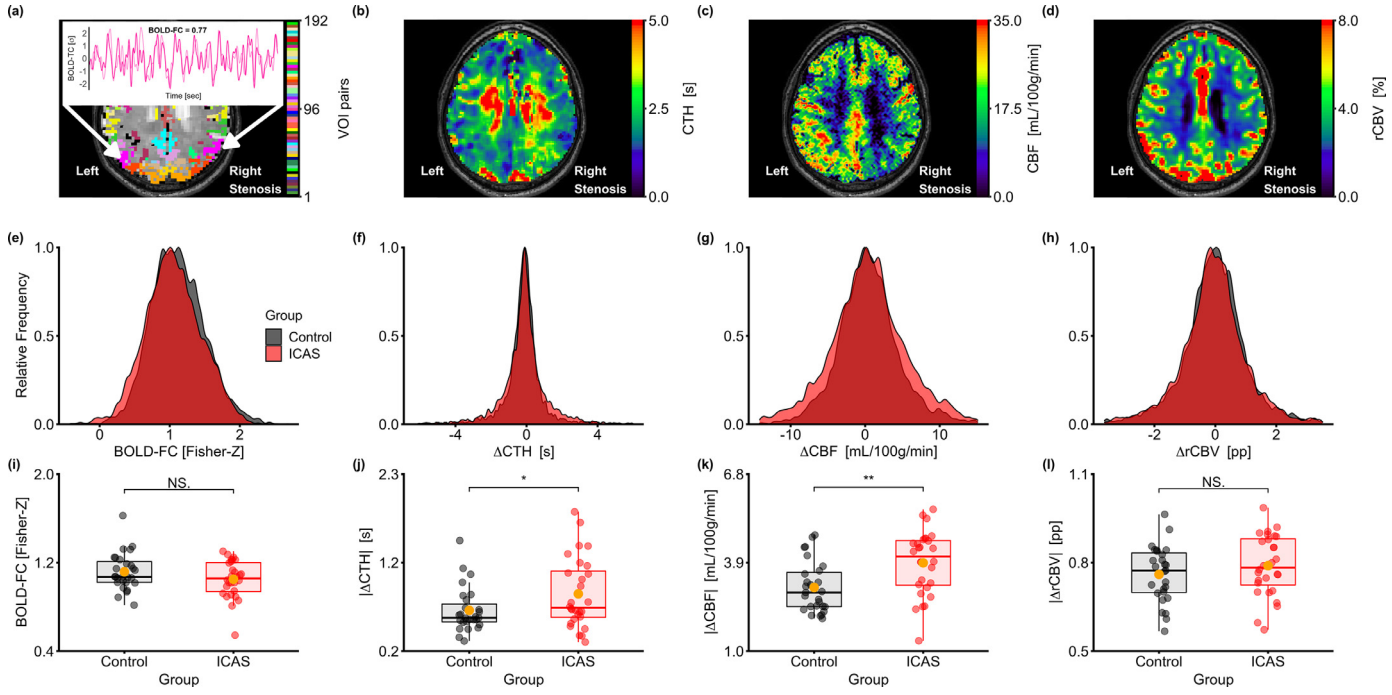

Fig. 2. AICHA VOIs (a), exemplary NVC parameter maps of one ICAS patient (b-d), sample distributions (e-h) and group differences (i-l) in BOLD-FC and NVC parameters. (a) Brain parcellation according to the AICHA atlas with an insert depicting two exemplary BOLD-TCs of homotopic regions, whose Pearson's correlation reflects homotopic BOLD-FC, (b-d) exemplary parameter maps of CTH (b), CBF (c) and rCBV (d) for a selected slice of an ICAS patient with a right-sided stenosis. (e-h) Frequency distributions of BOLD-FC (e) between pairwise homotopic VOIs and corresponding ΔCTH (f), ΔCBF (g) and ΔrCBV (h) across all VOI pairs of asymptomatic ICAS patients and healthy controls. Relative frequency of measured values are indicated in grey for healthy controls and in bright red for ICAS patients. Dark red color indicates overlap between groups. (i-l) Paired scatterplots of BOLD-FC (i) as well as |ΔCTH| (j), |ΔCBF| (k) and |ΔrCBV| (l) between pairwise homotopic VOIs averaged across 192 VOI pairs for each participant. In each panel, one dot represents one participants' average value, where red indicates ICAS patients and black healthy control participants. Thick horizontal bars indicate median values for each group, upper and lower borders of the square indicate the 75% (third quartile) and 25% (first quartile) percentile, respectively. Vertical lines indicate the 1.5 times interquartile range (between first and third quartile). Orange dots indicate the respective group mean. Global group differences regarding the respective variables were examined with Welch's t-test, significant group differences are indicated with asterisks (* for $p < 0.05$, ** for $p < 0.01$), non-significant differences with NS. Abbreviations: AICHA, Atlas of Intrinsic Connectivity of Homotopic Areas; BOLD-FC, blood oxygenation level dependent functional connectivity; CBF, cerebral blood flow; CTH, capillary transit time heterogeneity; rCBV, relative cerebral blood volume; ICAS, internal carotid artery stenosis; NVC, neuro-vascular coupling; VOI, volume of interest.

d for a selected slice of an asymptomatic ICAS patient with a right-sided stenosis. The distribution of homotopic pairwise BOLD-FC, as well as pairwise ΔCTH, ΔCBF, and ΔrCBV are depicted in Fig. 2e-h for both asymptomatic ICAS patients and healthy controls across 192 region pairs, approximating normal distributions in all cases. As these distributions suggest marked group differences, we conducted an additional group comparison analysis for individually averaged outcomes, i.e., BOLD-FC, |ΔCTH|, |ΔCBF| and |ΔrCBV|, respectively. At $p < 0.05$, Welch's t-testing revealed comparable BOLD-FC and |ΔrCBV| for ICAS patients and controls, but significantly larger side differences for |ΔCTH| and |ΔCBF| in patients (Fig. 2i-l). Albeit ICAS patients exhibited stronger side differences, significant pairwise differences between homotopic areas were detected for both the patients and healthy controls in all three NVC parameters, namely |ΔCTH|, |ΔCBF|, and |ΔrCBV| (group-wise one-sample t-tests at $p < 0.05$; control group, $p < 0.0001$; ICAS group, $p < 0.0001$).

With regard to regional differences across brain regions, an additional analysis identified specific regions with group differences for BOLD-FC, |ΔCTH|, |ΔCBF| and |ΔrCBV|, respectively, such as fusiform sulcus or supramarginal gyrus (see supplementary Fig. S1). Regions with significant differences in |ΔCTH| and |ΔCBF| partially overlapped but to a lesser degree with BOLD-FC. To allow a better assessment of anatomic localization, regions showing significant differences (at $p < 0.05$ uncorrected) are shown as color overlay in supplementary Fig. S2. Furthermore, we found a weak but significant correlation between |ΔCBF| and the degree of stenosis in ICAS patients (see supplementary Figure S3).

Influence of CTH and further NVC parameters on BOLD-FC: To test our hypothesis that CTH influences BOLD-FC, we performed an LMM analysis with pairwise BOLD-FC as dependent variable and pairwise |ΔCTH| as independent variable of interest. We further included |ΔCBF| and |ΔrCBV| as independent variables in order to both control for their effects on BOLD-FC and to study their influence on BOLD-FC. In addition, age was included to control for systemic age-related deviations. With regard to random effects, the slope of |ΔrCBV| had to be excluded because its variation among participants was close to zero, thus prohibiting a model fit (singular fit). Overall 8716 observations were included in the model, distributed across the 55 participants. Results are summarized in Table 3 and Fig. 3.

(i) *BOLD-FC*, i.e., pairwise BOLD-FC without differences in hemodynamic parameters between homotopic VOI pairs, was at z = 1.16 (corresponding to Pearson's r = 0.82; 95% CI: 1.11 to 1.21) across participants, indicating high levels of homotopic functional connectivity. The two groups, ICAS patients and healthy controls, did not significantly deviate from this average in terms of group difference.

(ii) *Significant group-wise, fixed effects of NVC parameters on BOLD-FC* were found for both |ΔCTH| and |ΔCBF| across both groups. More specifically, BOLD-FC decreased with increasing |ΔCTH| and |ΔCBF|.

a) For |ΔCTH|, BOLD-FC was estimated to decrease on average by −0.12 (95% CI: −0.15 to −0.09; −10% from baseline) per 1 σ of |ΔCTH| (i.e., 2.47 s) between homotopic VOIs. This effect was significantly different between both groups, as demon-

Table 3
Summary of fixed effects for linear mixed model, LMM, analysis.

	BOLD-FC			
Regressors	*Estimates*	*CI*	*Statistic*	*p*
(Intercept)	1.16	1.11 to 1.21	44.91	**<0.001**
cAge	0	−0.01 to 0.01	0.85	0.4
|ΔCTH|	−0.12	−0.15 to −0.09	−7.67	**<0.001**
|ΔCBF|	−0.05	−0.08 to −0.03	−4.03	**<0.001**
|ΔrCBV|	0	−0.02 to 0.01	−0.23	0.82
cAge * |ΔCTH|	0	−0.00 to 0.01	1.58	0.12
cAge * |ΔCBF|	−0.01	−0.01 to −0.00	−2.2	**0.03**
cAge * |ΔrCBV|	0		−1.24	0.22
Group [ICAS]	−0.02	−0.07 to 0.03	−0.68	0.5
Group [ICAS] * cAge	−0.01	−0.02 to 0.00	−1.38	0.17
Group [ICAS] * |ΔCTH|	−0.04	−0.07 to −0.01	−2.64	**0.01**
Group [ICAS] * |ΔCBF|	0	−0.02 to 0.03	0.05	0.96
Group [ICAS] * |ΔrCBV|	0.01	−0.01 to 0.02	0.64	0.53
Group [ICAS] * cAge * |ΔCTH|	0	−0.01 to 0.00	−0.79	0.43
Group [ICAS] * cAge * |ΔCBF|	0.01	0.00 to 0.01	2.51	**0.01**
Group [ICAS] * cAge * |ΔrCBV|	0		0.2	0.84

Note: Under 'Regressors', the variables incorporated in the model are listed. Categorical variables were deviation coded (Group: ICAS = 1, Controls = −1). Age was centered on the median age in the sample (participants with a median age equal 0 in the coding). The intercept estimate describes average BOLD-FC when all other predictor variables are 0, i.e. for all included participants of median age. Estimates for other variables indicate the estimated change in BOLD-FC should the predictor value increase by 1 σ (e.g. a decrease of BOLD-FC by −0.12 for every 2.47 seconds CTH difference between the respective VOIs). Interactions between participant group and predictors are indicated by an asterisk, with the respective Group in square brackets. Confidence intervals for the estimates are indicated by CI. If no CI is indicated this means that the effect was always smaller than 0.001. The test statistic is derived from a one-sample t-test, against the null-hypothesis that the estimate does not differ significantly from 0. Effects for the healthy control group are identical to those of ICAS patients, except being reversed in polarity (Group coding for healthy participants = −1). Abbreviations: BOLD-FC, blood oxygenation level dependent functional connectivity; CBF, cerebral blood flow; CTH, capillary transit time heterogeneity; rCBV, relative cerebral blood volume; ICAS, internal carotid artery stenosis.

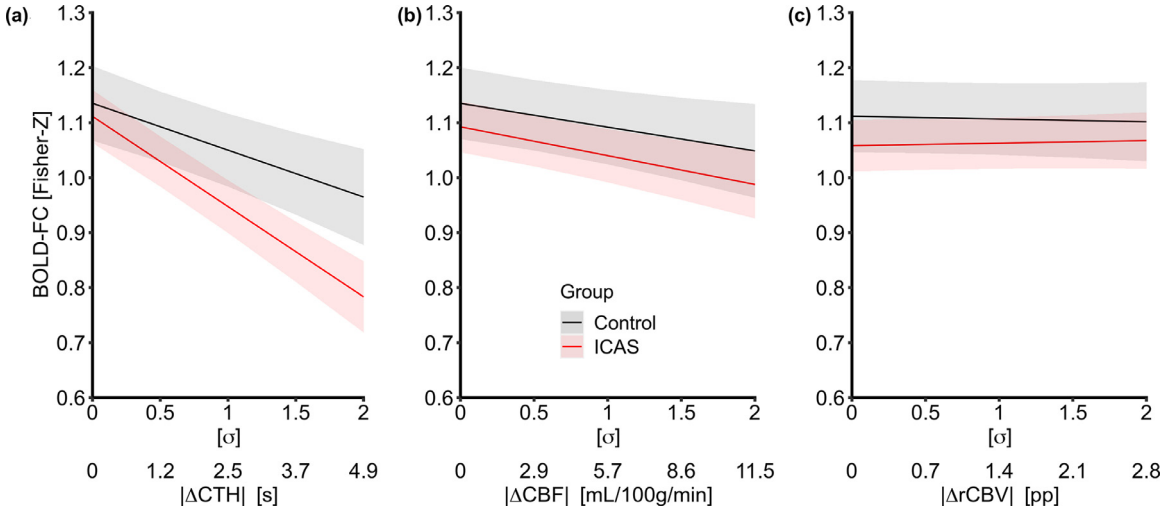

Fig. 3. Group effects of NVC parameters on BOLD-FC. Slopes indicate predicted changes in BOLD-FC (y-axis) with increasing |ΔCTH| (a), |ΔCBF| (b) and |ΔrCBV| (c) between pairwise VOIs for ICAS patients (red) and controls (black). The group-wise intercepts indicate the individually estimated baseline BOLD-FC for VOI pairs without difference in the respective NVC metric. Shaded areas indicate the 95% confidence interval of the predicted values. Abbreviations: BOLD-FC, blood oxygenation level dependent functional connectivity; CBF, cerebral blood flow; CTH, capillary transit time heterogeneity; rCBV, relative cerebral blood volume; ICAS, internal carotid artery stenosis; NVC, neuro-vascular coupling; VOI, volume of interest.

strated by a significant interaction of CTH and group (see Fig. 3a and Table 3 – Group [ICAS]*|ΔCTH|). Quantitatively, the decrease was significantly stronger for ICAS patients (−0.16; 95% CI: −0.19 to −0.13; -14% from baseline) than for the control group (−0.08; 95% CI: −0.11 to −0.05; −7% from baseline). These effects were only slightly altered by age for female participants (for details see Table S1 & Supplementary Results – Influence of sex differences). The effect of |ΔCTH| on BOLD-FC was furthermore dependent on the participants' baseline BOLD-FC. More specifically, higher baseline values indicated stronger BOLD-FC decrease with |ΔCTH| (r = −0.51).

b) For |ΔCBF|, BOLD-FC was estimated to decrease on average by −0.05 (95% CI: −0.08 to −0.03; −4% from baseline) per 1 σ of |ΔCBF| (i.e., 5.72 ml/100 g/min; see Fig. 3b and Table 3 – |ΔCBF|). While there were no group specific effects of |ΔCBF|, age had a small but significant interacting influence, i.e., the decrease was slightly stronger in participants older than the median age of 71 years (an additional −0.01 per year; see Table 3 – cAge * |ΔCBF|) and vice versa for participants younger than median age. This effect was stronger for participants in the control group (additional −0.01, i.e. −0.02 per year) and almost vanished for the ICAS patients (additional +0.01, i.e., 0 per year; see Table 3 –

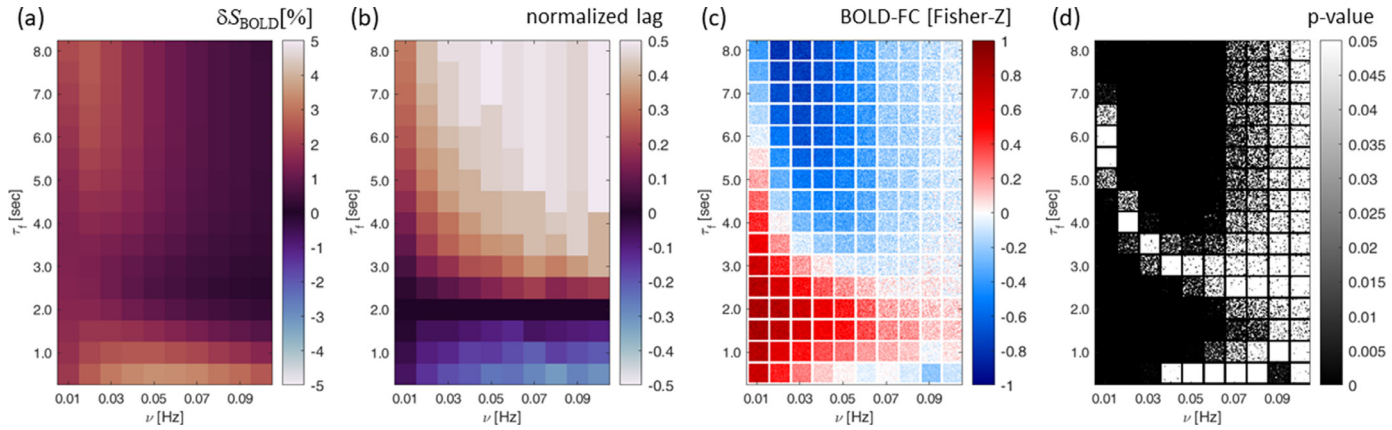

Fig. 4. Matrix representations of BOLD-TC peak-to-peak amplitudes (a), normalized temporal lags (b), BOLD-FC (c) and corresponding p-values (d) across the range of investigated CBF characteristic time constants τ_f and neuronal input frequencies ν. (a) Peak-to-peak amplitudes and (b) normalized temporal lags were determined from noise free resting state portions of the simulated BOLD-TCs (last 200 s) yielding one value per simulated (τ_f, ν) scenario. At each neuronal input frequency, the temporal lags between the respective reference BOLD-TC (framed in yellow at τ_f = 2.0 s) and the target BOLD-TCs with τ_f = [0.5 … 8.0] sec were determined via cross correlation and normalized by the period of the neuronal input frequency, resulting in normalized lags between −0.5 and 0.5. (c) BOLD-FC and (d) *p*-values values at each neuronal input frequency were obtained by calculating Z-transformed Pearson's correlation coefficients between the resting portions (last 200 s) of the selected reference seed BOLD-TC (framed in yellow at τ_f = 2.0 s) and the target BOLD-TCs across the entire range of BOLD-TCs with τ_f = [0.5 … 8.0] s. Insignificant correlations (at $p < 0.05$) appear white in panel (d). Individual squares in panels (c) and (d) appear noisy because the seed and target BOLD-TCs were complemented with random white noise prior to BOLD-FC calculation achieving SNR_0 = 250 in the baseline portions of the signal. 16 × 16 different random white-noise realizations were used for each pair of investigated parameter values, constituting the individual squares in panels (c) and (d). Abbreviations: δS_{BOLD}: percentage peak-to-peak BOLD amplitude.

Group [ICAS] * cAge * |ΔCBF|). Comparison of overall effect sizes of |ΔCTH| and |ΔCBF| revealed that the BOLD-FC reduction due to increases in |ΔCTH| were significantly stronger than the ones caused by baseline CBF (Welch's t-test of participants estimated individual slopes; t = −3.1, $p < 0.05$). The detrimental effects of CTH and CBF differences were furthermore robustly linked, as indicated by their strong correlation (r = 0.66; see Table S2).

c) For |ΔrCBV|, we did not found any effect on BOLD-FC (see Fig. 3c).

d) Regarding model explanatory power, the estimated R^2 value for the model was 0.23 (based on Nakagawa and Schielzeth (2013)) when accounting for the variation of participants among the estimated group based effects of hemodynamic parameters (for detailed random effects results see Table S2 & Supplementary Results – Random Effects).

3.2. Simulation results regarding the influence of CBF response timing on pairwise BOLD-FC

In order to facilitate understanding of how BOLD-FC depends on CBF response timing, results of BOLD-FC simulations are presented together with analyses of BOLD-TC characteristics. Fig. 1e illustrates the relation for a neuronal input frequency of ν = 0.05 Hz. Compared to the healthy reference BOLD-TC simulated with τ_f = 2.0 s (depicted in blue), faster CBF responses (τ_f < 2.0 sec, depicted in light grey) elicit higher BOLD signal changes and the periodic BOLD-TC signal is shifted to the left, corresponding to negative temporal lags. Slower CBF responses (τ_f > 2.0 s, depicted in dark grey) on the other hand, cause positive temporal lags (i.e., signal shifts to the right) and less pronounced influence on ΔS_{BOLD}. Simulation results for the whole range of 16 characteristic CBF time constants (τ_f = [1.0,…, 8.0] s, vertical axis) and ten neuronal input frequencies (ν = [0.01,…, 0.1] Hz, horizontal axis) are summarized via color-coded BOLD-TC amplitudes (Fig. 4a), temporal lags (Fig. 4b), and finally BOLD-FC (Fig. 4c) together with corresponding *p*-values (Fig. 4d).

Significantly positive BOLD-FC is observed in the lower left quarter of Fig. 4c, where τ_f (for each investigated frequency), ranges around the healthy reference value (τ_f = 2.0 s, framed in yellow). For the lowest investigated frequency (ν = 0.01 Hz), positive BOLD-FC values range up to τ_f = 5.5 s, though with vanishing statistical significance (Fig. 4d). With increasing neuronal input frequency, the range of positive BOLD-FC drastically narrows to τ_f = [1.0, …, 2.5] s at ν = 0.06 Hz, while at ν = 0.07 Hz and above, *p*-values indicate that correlations are no longer significant (Fig. 4d). Significantly positive BOLD-FC goes along with BOLD signal amplitudes similar to the reference (framed in yellow, Fig. 4a) and small positive or negative temporal lags compared to the reference (framed in yellow, Fig. 4b).

Significantly negative BOLD-FC is observed for longer characteristic time constants, being separated from the realm of positive BOLD-FC by a transition zone of vanishing BOLD-FC (Fig. 4c). The location of this transition zone is frequency dependent, it occurs at τ_f = 6.0 s for ν= 0.01 Hz and drops to τ_f = 3.0 s for ν= 0.07 Hz. At 0.07 Hz and above, negative BOLD-FC is hardly significant (Fig. 4d). Significantly negative BOLD-FC goes along with BOLD signal amplitudes rather higher than the reference (framed in yellow, Fig. 4a) and large positive temporal lags compared to the reference (framed in yellow, Fig. 4b). Weakly significant negative BOLD-FC could also occur for very fast CBF responses (τ_f = 0.5 s) at high neuronal input frequencies (ν= 0.09 Hz).

Together with information on timing aspects of the CBF response as obtained by the empirical analysis of multi-parametric MRI data, these BOLD-FC matrices can be used to interpret and explain empirical BOLD-FC results.

4. Discussion

In order to test the hypothesis that capillary transit time heterogeneity, CTH, influences BOLD-FC and may serve as an indicator for broadened and delayed CBF responses, we used a combined empirical and theoretical approach. (i) Our empirical analysis of multi-parametric hemodynamic MRI data of asymptomatic high-grade unilateral ICAS patients and healthy controls demonstrates significant reductions of BOLD-FC with increasing CTH differences between homotopic brain areas that were significantly more pronounced in ICAS patients. Crucially, due to largely preserved neuronal functioning in asymptomatic ICAS, our results demonstrate that CTH differences between homotopic brain areas can explain BOLD-FC reductions independent from changes in neuronal activity. (ii) Our theoretical simulation-based approach revealed that an

increase in the characteristic time constant τ_f of blood flow responses induces delays and broadening of the CBF response, which in turn is associated with significant changes in BOLD-FC, including sign shifts from positive to negative. (iii) Linking empirical and theoretical findings, simulation results of BOLD-FC variability as a function of CBF response timing variability fit our empirical findings of CTH impact on BOLD-FC, suggesting that CTH may serve as an indicator of CBF response timing.

This is the first study demonstrating local CTH impacts on BOLD-FC in humans. Furthermore, we offer for CTH a distinct hemodynamic interpretation in terms of local perfusion temporal response characteristics. In summary, results suggest that perfusion response delay and broadening impact on BOLD-FC independently from neuronal changes.

4.1. Empirical findings reveal NVC impact on BOLD-FC

4.1.1. CTH and its impact on BOLD-FC

We observed that BOLD-FC is significantly predicted by CTH differences between homotopic cortical VOI pairs. Specifically, BOLD-FC correlations between homotopic brain regions' BOLD-TCs decreased when |ΔCTH| increased (Fig. 3a). Moreover, the observed effect was both significantly stronger in patients with ICAS than healthy controls and independent of age.

Physiologically, CTH describes the distribution of red blood cell capillary transit times, where an increase in CTH corresponds to a broadening of this distribution (Jespersen and Ostergaard, 2012). Based on relations between distributions of relative flow rates and capillary transit times (Østergaard et al., 1999), we assume that such broadening necessarily also causes a delayed CBF response, which lead us to propose CTH as a marker for τ_f (see rationale in section '2.2. Theoretical considerations regarding the link between CTH and CBF response'). In previous simulation studies, it has already been demonstrated that CTH influences CBF and BOLD responses to brain activation (Rasmussen et al. 2015; Angleys et al., 2019), yielding results consistent with experimental findings in small animal studies (Rasmussen et al. 2015). The influence of CTH on BOLD-FC has not yet been examined in human rs-fMRI studies so far but CTH increases have been demonstrated in neurodegenerative and vascular diseases (Kaczmarz et al., 2021; Mundiyanapurath et al., 2016; Nielsen et al., 2020; Potreck et al., 2019). Furthermore, there is some evidence that CTH eventually impedes cerebral oxygen supply in neurodegenerative and vascular diseases (Arsava et. al., 2018; Ostergaard et al., 2013a; Ostergaard et al., 2016; Ostergaard et al., 2013b).

In our patients with asymptomatic ICAS, elevated CTH in the hemisphere ipsilateral to the stenosis is not accompanied by alterations in oxygen extraction fraction (OEF) (Kaczmarz et al., 2021; Figs. 3 & 4). Furthermore, CBF and $CMRO_2$ ipsilateral to the stenosis are comparable to healthy controls, while contralateral values are significantly higher in ICAS patients (see Fig. 3 of (Gottler et al., 2019a; Gottler et al., 2020)). In the healthy subjects of our study cohort, we did not find general hemispheric CTH differences, in line with their overall intact perfusion status (Kaczmarz et al., 2021), but detailed regional analysis revealed that CTH differences between homotopic regions nevertheless exist across the brain – even though to a lesser degree than in asymptomatic ICAS patients (Fig. 2f, j; see supplementary Figs. S1 & S2 for detailed regional analysis). Accordingly, the CTH effect on BOLD-FC for the healthy participant group might be underestimated, explaining the significant interaction between group and |ΔCTH| on BOLD-FC. Nevertheless, systematic group differences in the relation between |ΔCTH| and BOLD-FC exist, possibly due to intact compensatory mechanisms in the healthy vascular-hemodynamic system. Cerebrovascular reactivity could be a potential candidate for such a compensatory mechanism, as impaired CVR has also been shown in our cohort of asymptomatic ICAS patients (Kaczmarz et al., 2021). Interestingly, CVR is not only reduced ipsilateral to the stenosis compared to the unaffected contralateral side, but also bilaterally compared to healthy controls (see Fig. 3 in Kaczmarz et al., 2021). Since an intact CVR is necessary for healthy blood flow responses to increased neuronal activity (D'Esposito et al., 2003; De Vis et al., 2018; Lewis et al., 2020; Mark et al., 2015; van Niftrik et al., 2019), weak physiological differences in CTH might be compensated by an intact CVR.

The question of which possible hemodynamic and physiological processes might underpin the effect of CTH increases on BOLD-FC decreases will be discussed below using our simulation results for interpretation.

4.1.2. Baseline perfusion, namely CBF and rCBV, and its impact on BOLD-FC

Reductions in BOLD-FC were also related to increasing cross-hemispheric differences in local baseline CBF (Fig. 3b) but not to differences in rCBV (Fig. 3c). In contrast to CTH, there were no ICAS group specific effects of |ΔCBF| on BOLD-FC, but age had a small and significant effect. In our cohort of asymptomatic ICAS patients, increases in |ΔCBF| and |ΔrCBV| correspond to reduced CBF and increased CBV ipsilateral to the stenosis (see Fig. 3 in (Kaczmarz et al., 2021)). The ICAS patients' average |ΔCBF|, but not |ΔCTH| and |ΔrCBV|, increased weakly but significantly with the degree of stenosis (see supplementary Fig. S3). Since hemodynamic impairments strongly depend on the individual vascular anatomy, mainly collateral flow across the circle of Willis (Richter et al., 2017; Kaczmarz et al., 2019), this weak dependence fits our expectation. In ICAS patients, reductions in microvascular perfusion (i.e., baseline CBF) and accompanying, compensatory increases in rCBV ipsilateral to the stenosis (Kaczmarz et al., 2021) are supposed to result from a reduced cerebral perfusion pressure (Powers et al., 1987; Schroeder, 1988). While our healthy controls do not show global baseline CBF and rCBV differences between hemispheres (Kaczmarz et al., 2021), our regional analysis still revealed small but significant pairwise differences for baseline CBF (Fig. 2g,k) and rCBV (Fig. 2h,l), albeit to a significantly lower degree as compared to ICAS patients (see supplementary Figures S1 & S2 for a detailed regional analysis).

Concerning the significant influence of baseline CBF on BOLD-FC, our result is in line with several previous findings. For example, BOLD-FC was found to be significantly correlated with regional baseline CBF in functional brain network hubs (Liang et al., 2013) and coupled to regional baseline CBF (Li et al., 2012). Using a scaling approach, first proposed by (Qiu et al., 2017), (Champagne et al., 2020) demonstrated recently that accounting for regional differences in baseline CBF reduced the difference in BOLD-FC patterns observed between patients with mild traumatic brain injury and healthy controls.

Concerning the relatively stronger |ΔCTH| than |ΔCBF| effect on BOLD-FC, our results suggest a link among previously separate findings. In patients with Alzheimer's disease, not only aberrant CTH has been demonstrated (Nielsen et al., 2020; Ostergaard et al., 2013a), but also an impact of reduced baseline CBF on BOLD-FC (Gottler et al., 2019b). In ICAS patients, we similarly found aberrant CTH and impact of reduced baseline CBF on BOLD-FC but also increased rCBV (see Fig. 3 in (Kaczmarz et al., 2021)). Thus, we suggest more generally, that brain disorders of subtle but chronic hypo-perfusion, which are likely accompanied by chronic compensatory vasodilation, are at higher risk for CTH alterations. Based on our results of relatively smaller effects of |ΔCBF] compared to |ΔCTH|, the relevance of CTH alterations seems to be higher for BOLD-FC, than the influence of baseline perfusion. This might be explained by an inherently larger extent of CTH changes than those of baseline CBF and compensatory rCBV changes. This explanation is inspired by our finding in unilateral asymptomatic ICAS patients, namely that CTH increases ipsilateral to the stenoses are much more widespread than alterations of baseline CBF and rCBV, which are more focused to vascular border zone areas (Kaczmarz et al., 2021). In any case, the simultaneous and strongly correlated impact of both CTH and baseline CBF on BOLD-FC accords with an inherent link between these variables (Jespersen and Ostergaard, 2012).

Finally, the small moderating effect of age on the influence of CBF, with stronger effects in healthy older subjects, could hint at a loss of compensatory factors countering the detrimental effects of CBF differ-

ences with progressing age. Given the widespread impact of age on various hemodynamic-vascular processes and thus NVC (Beishon et al., 2021), a larger moderating effect could be expected in a sample with a larger age range. The negligible effect of age among ICAS patients on the other hand, fits with our assumption of already depleted compensatory factors.

4.2. Simulations reveal CBF timing impact on BOLD-FC

Our simulations of BOLD-FC across a range of characteristic time constants τ_f demonstrates the dependency of BOLD-FC on delayed and broadened CBF responses. For a purely sinusoidal neuronal input of 0.05 Hz, we found diminished BOLD-FC for characteristic CBF time constants deviating more than a second from the healthy reference at $\tau_f = 2$ s. Regarding slower CBF responses, BOLD-FC is already clearly reduced for $\tau_f = 2.5$ s, turning largely insignificant for $\tau_f = 3.0$ s, and finally getting negative for $\tau_f > 3.0$ s (see Fig. 4c & d). This behavior can be well explained by an increasingly positive lag with increasing τ_f, where bright colors in Fig. 4b indicate that the target BOLD-TCs for $\tau_f > 6.5$ s are almost in opposite phase to the reference BOLD-TC (at $\tau_f = 2.0$ s).

The result of diminished BOLD-FC fits with our empirical results as well as with a number of rs-fMRI studies that demonstrated decreased rs-fMRI-based BOLD functional connectivity in patients with vascular diseases including ICAS (Avirame et al., 2015; Chang et al., 2016b; Cheng et al., 2012; Lin et al., 2014; Wang et al., 2017), but also in neurodegenerative diseases, depression and schizophrenia (Brandl et al., 2019; Manoliu et al., 2014; Zhou et al., 2010; Zhou and Seeley, 2014). All these disorders have also been associated with perfusion deficits (Gottler et al., 2020; Gottler et al., 2019b; Kaczmarz et al., 2021; Katsel et al., 2017; Love and Miners, 2016). In addition and highly interestingly, negative BOLD-FC has been observed in a range of different brain disorders from Alzheimer's disease or Frontotemporal Dementia (Nuttall et al., 2016; Zhou et al., 2010) to schizophrenia (Damaraju et al., 2014; Manoliu et al., 2014), all of which have been associated with significant perfusion deficits (Katsel et al., 2017; Love and Miners, 2016). Typically, negative BOLD-FC has been explained by potential effects of either global signal changes (Chang et al., 2016a; Scholvinck et al., 2010; Turchi et al., 2018) or problematic preprocessing of rs-fMRI data with respect to the global grey matter BOLD signal such as global signal regression (Liu et al., 2017; Murphy and Fox, 2017; Power et al., 2012; Siegel et al., 2014). However, our simulation results shed new light on that issue, offering effects of impaired neurovascular coupling, such as local perfusion delays, as a possible explanatory mechanism for the emergence of negative BOLD-FC. Thus moving the field forward in the understanding of a phenomenon that has proven challenging and has thus been largely ignored so far.

Exploring the frequency dependence of BOLD-FC, we performed simulations for neuronal inputs between 0.01 Hz and 0.1 Hz (Fig. 4). Again, observed BOLD-FC changes at different input frequencies ν can be explained by the interplay of changing peak-to-peak amplitudes (Fig. 4a) and temporal lags/phase shifts (Fig. 4b). Areas of diminished BOLD-FC (in the (τ_f, ν) parameter space) either overlap with areas of low to vanishing BOLD-TC amplitudes (see Fig. 4a) or coincide with relevant lags (see Fig. 4b). Strong positive BOLD-FC (Fig. 4c) is observed where high peak-to-peak amplitudes coincide with temporal lags around zero, indicating that the BOLD-TCs of seed and target regions are in phase. Significantly negative BOLD-FC values are observed in parts of the parameter space, where the BOLD-TCs are shifted by about half a period where the BOLD-TCs in the seed and target region are roughly in opposite phase. Remarkably, the area with low and diminished BOLD-FC in the parameter space extends with increasing input frequency and shrinks with decreasing input frequency, compared to the middle input frequency of 0.05 Hz (see Fig. 4c). This finding implies a filter effect of NVC, in a sense that low frequency neuronal input (< 0.05 Hz) appears more likely to produce positive BOLD-FC than high frequency neuronal input (> 0.05 Hz). This simulation-based finding fits very well with a recent experimental observation (Siegel et al., 2016). In a cohort of patients with subacute stroke, the authors found a decrease of BOLD signal power with frequency in non-lesioned brain areas that exhibited significant lags in the BOLD signal. Interestingly, brain areas without and with lag, respectively, showed comparable BOLD signal power between 0.01 and 0.04 Hz. At higher frequencies (0.04 to 0.09 Hz) the overall power decreased, but was significantly lower in areas exhibiting a lag in BOLD signal (see Fig. 2 in (Siegel et al., 2016)). This finding provides evidence for a low pass filter effect of NVC whose efficiency increases in the presence of perfusion delays. However, it has to be noted that Siegel et al. investigated the dependence of BOLD-FC on systemic BOLD signal time lags instead of timing aspects of local NVC as in our current study. However, systemic perfusion delays are well known to occur in vascular diseases, as is the case in our cohort of asymptomatic ICAS patients (Kaczmarz et al., 2021). Thus, further studies are clearly needed to disentangle the effects of local and systemic perfusion delays.

4.3. Linking empirical and simulation results of local NVC impact on BOLD-FC

4.3.1. CTH and CBF responses

As outlined in methods section '2.2. Theoretical considerations regarding the link between CTH and CBF response', we suggest that increased CTH could serve as a marker for broadened and delayed CBF responses. Based on this kind of 0^{th}-order approximation, the simulation model might help us to understand how timing aspects of the CBF response influence BOLD-FC. In accordance with previous work, we assumed a normal $CMRO_2$ response with $\tau_m = 2$ sec (Archila-Melendez et al., 2020). An equally fast and narrow CBF response with $\tau_f = 2$ s causes a positive BOLD signal change when the delivery of oxygen surpasses its consumption. In our simulations, this condition is well met by assuming CBF and $CMRO_2$ response amplitudes of 50% and 25%, respectively. When the CBF response is now delayed and broadened – while keeping the absolute amount of delivered blood constant – the delivery of oxygenated blood is stretched across a longer period of time, resulting in a diminished short-term delivery of oxygen and in turn, a diminished positive BOLD response. With increasing τ_f, the peak CBF response is increasingly delayed and the maximum amplitude diminished so that at a certain point, the oxygen consumption, i.e., the simulated normal $CMRO_2$ response, surpasses the oxygen delivery, eventually resulting in an increase of deoxyhemoglobin and thus a negative BOLD response and consequently also a negative BOLD-FC. The point in parameter space where exactly this happens depends on the frequency of the neuronal input (see Fig. 4c) but also on the assumptions with regard to the reference seed.

In general, our empirical finding of decreasing BOLD-FC with increasing $|\Delta CTH|$ between VOI pairs, fits very well with our simulation result of decreasing BOLD-FC with increasing τ_f, particularly if one accepts a link between CTH and CBF response timing. As discussed above, in our sample of asymptomatic ICAS patients, an increase in $|\Delta CTH|$ corresponds to CTH increases ipsilateral to the stenosis. As the reference seed BOLD-TC was chosen to represent a 'healthy' NVC response, BOLD-FC values with increasing τ_f correspond to situations with increasingly delayed and broadened CBF responses in an impaired target region. This corresponds to the situation in our asymptomatic ICAS patients, where CTH is increased in VOIs ipsilateral to the stenosis compared to the contralateral (healthy) VOIs. As we can see in Fig. 4 across the range of simulated frequencies, BOLD-FC decreases with increasing τ_f across the entire range of simulated frequencies, which perfectly fits our empirical results, where we found that unilateral CTH increases cause decreases in pairwise homotopic BOLD-FC. Thus, it appears plausible to consider CTH as an indicator for the CBF response's characteristic time constant τ_f, where $|\Delta CTH|$ roughly relates to differences in characteristic time constants τ_f, which causes phase shifts and amplitude modulations between BOLD-TCs in paired homotopic VOIs. BOLD-FC between pairwise

VOIs is in turn diminished even though neural activity is most likely largely comparable across homotopic VOI pairs as discussed above.

As indicated by our empirical analysis, BOLD-FC is also influenced by baseline values of CBF. However, baseline CBF is not explicitly considered in our simulation approach. All changes are simulated relative to a normalized baseline. What actually matters are the changes relative to this baseline, and in this respect, it would be important to know if and how baseline CBF influences the CBF response amplitude. Since increased rCBV as well as reduced CVR have been detected in our cohort of asymptomatic ICAS patients (Kaczmarz et al., 2021), it is likely that reduced baseline CBF is often accompanied by a reduced CBF response amplitude, which according to our previous simulations also predicts reduced BOLD-FC (Archila-Melendez et al., 2020). However, one should be aware that this is not necessarily the case (Powers et al. 1988; Siero et al., 2015; Amemiya et al. 2012).

With respect to rCBV, our empirical analyses did not show a significant influence. This again fits with our simulations because the assumed slow CBV response acts to dampen the influence of CBV in the presence of fast oscillatory neuronal activity as can be seen in Fig. 1b and has been discussed in detail previously (Archila-Melendez et al., 2020).

4.3.2. Pathophysiology of local NVC in ICAS and its impact on BOLD-FC

The ICAS patients included in our study showed mild to moderate capillary dysfunction, which, beyond increases in CTH, manifested in reduced baseline CBF and CVR as well as elevated rCBV (Kaczmarz et al., 2021) with ipsilateral $CMRO_2$ comparable to healthy controls (Gottler et al., 2019a). Mean grey matter CTH was found to be about 2.8 s in healthy elderly (Kaczmarz et al., 2021), and mean CTH differences between VOI pairs are about 0.9 s and 0.7 s for ICAS patients and healthy controls, respectively (with a small fraction of VOIs showing lager $|\Delta CTH|$ values up to $\approx$ 3 s). These values indicate that in the majority of voxels pathological CBF responses in ICAS patients do not differ too much from the reference seed assumed in our simulation approach. This means that the simulated τ_f range exceeds the pathophysiological range in ICAS patients by far.

The reduction in baseline CBF certainly also plays a role, especially in combination with the observed ipsilateral rCBV increase, indicating potentially chronic compensatory vasodilation and simultaneously reduced CVR, which has indeed been demonstrated on group level (Kaczmarz et al., 2021). According to our previous simulation study (Archila-Melendez et al., 2020) and results from other groups (D'Esposito et al., 2003; Gottler et al., 2019b; Lewis et al., 2020; Mark et al., 2015; van Niftrik et al., 2019), intact CVR is an important prerequisite of BOLD fMRI studies not only in the resting state.

Finally, as CTH is expected to depend on baseline CBF (Jespersen and Ostergaard, 2012), ICAS patients might also be affected from an inability to reduce CTH in response to neuronal activity that has been observed in animal studies (Jespersen and Ostergaard, 2012; Kleinfeld et al., 1998; Schulte et al., 2003; Stefanovic et al., 2008).

4.4. Limitations

There are several shortcomings in our study, which have to be acknowledged. In the following, we list these limitations together with a brief discussion point-by-point.

Multi-parametric hemodynamic MRI: With respect to ASL, there are a number of known issues with regard to regional differences in arterial transit times, which potentially impede baseline CBF quantification with single-PLD ASL, especially in elderly subjects and patients with vascular diseases (Gottler et al., 2019a; Kaczmarz et al., 2021). We tried to minimize respective bias by using a PLD of 2000 ms as recommended (Alsop et al., 2015) and carefully checked data for arterial transit time artefacts (Kaczmarz et al., 2021). In addition, reduced labeling efficiency due to increased flow velocities in the stenosed vessel (Chen et al., 2017) as well as reduced compliance in patients could impact on CBF data quality. Furthermore, we included pCASL data with 2D EPI readouts in 15 subjects because pCASL with 3D GRASE readout was either not available (6 subjects) or rated of inferior quality. While these deviant data were distributed evenly between groups and a rating-based group comparison of CBF data quality (data not shown) does not indicate significant group differences, we cannot exclude that measurement accuracy and SNR could potentially influence the results of our analyses. Similarly, there are a number of known issues with DSC MRI, starting from the valid definition of an arterial input function to potential influences of contrast agent leakage effects (Hedderich et al., 2019; Kluge et al., 2016). Likewise, CTH calculation relies on a number of assumptions that might not necessarily be fulfilled (Kaczmarz et al., 2021; Mouridsen et al., 2014). In addition, contrast agent application in itself is potentially problematic due to contrast agent accumulations (Kanda et al., 2015).

Analysis of BOLD-FC predictors: Since BOLD signal is well known to be confounded by numerous influences, we included several control variables in our analysis. Importantly, we included age because detrimental effects of age on BOLD-FC have been repeatedly demonstrated (Farras-Permanyer et al., 2019; Varangis et al., 2019) and sex because it has been found to influence cerebral blood flow and metabolism (Aanerud et al., 2017; Alisch et al., 2021; Daniel et al., 1989; Duque et al., 2017). An analysis regarding sex differences in CTH did not reveal significant effects in our subject cohort (data not shown). Other potentially confounding participant traits, e.g., hypertension or diabetes, were clearly associated with the grouping structure, i.e., more prevalent in ICAS patients (see Table 1), which prevented individual inclusion due to multicollinearity. Thus, we included the factor group as an overarching control variable, also to avoid fitting an overly complex model. While such variables could, therefore, have an individual impact on BOLD-FC or moderate the influence of NVC differences in BOLD-FC, the present study design is not suited to disentangle such individual effects. The larger impact of $|\Delta CTH|$ on BOLD-FC for ICAS patients could therefore also be related to additional factors associated with ICAS, beyond an impaired CTH. However, hypertension was found to be associated with both BOLD hyper-and hypo-connectivity only for few selected regions (Feng et al., 2020; Son et al., 2015; Carnevale et al., 2020). Blood pressure likewise has been found to only impair the BOLD signal under conditions of rapid change (Kalisch et al. 2001; Reimann et al., 2018). Even though CVR, besides CBF and CBV, is well known to influence the BOLD signal (Archila-Melendez et al., 2020) we decided not to include CVR for mainly two reasons: (1) sufficient quality breath-hold CVR data are only available from about two thirds of our study participants, (2) missing endtidal CO_2 data restrict analysis to purely qualitative statistical maps. However, the additional influence of CVR is an important factor that needs to be addressed in future studies.

Our model explains 23% of the BOLD-FC variance, clearly indicating that further factors impact BOLD-FC. Among these, cardiac and respiratory pulsations are best known (Beall and Lowe, 2007; Yoshikawa et al., 2020) but more recently, influence of systemic perfusion delays has also been demonstrated, e.g., in Moyamoya disease, stroke, stenosis patients and even healthy controls (Christen et al., 2015; Lv et al., 2013; Siegel et al., 2016; Tong et al., 2017; Tong et al., 2019). Beyond that, intrinsic local fluctuations in arteriole diameter, partially independent from resting-state neural activity, may drive blood flow oscillations and impact on BOLD-FC (Winder et al., 2017; Mateo et al., 2017). Likewise, the global brain signal, which we decided not to regress out certainly has an impact on BOLD-FC (Liu et al, 2017). Further factors include motion not detected by common motion regression procedures (Beall and Lowe, 2014). Lastly simply spontaneous differences in the underlying neuronal activity would lead to reduced BOLD-FC as well.

BOLD-FC modelling and the link between CTH and CBF response timing: A major strength of our simulation approach is that it allows detailed simulations regarding the impact of NVC impairments on BOLD-FC. The most important general issues about the validity of our approach have already been discussed (Archila-Melendez et al., 2020).

As outlined above, our simulations demonstrate that delayed and broadened CBF responses can explain reductions of BOLD-FC independent of reductions in neuronal activity. With regard to experimental evidence, we proposed a link between CTH increases and broadened and delayed CBF responses. This appears plausible on a qualitative level, however, for future studies, our simulation model clearly needs to be developed further. To establish a firm link between BOLD-FC and measurable physiological parameters in humans, an improved model needs to consider the interplay of MTT, CTH, CBV and CBF (Østergaard et al., 1996; Østergaard et al., 1999) as well as the complexities introduced by the effects of CTH on brain oxygenation (Jespersen and Østergaard, 2012) and in particular BOLD responses (Rasmussen et al., 2015; Angleys et al., 2018). Moreover, the influence of the baseline physiology has been neglected in this study because OEF was unimpaired in our sample of asymptomatic ICAS patients (Kaczmarz et al., 2021) and statistical analysis did not indicate influence of CBV (Fig. 3c). However, future studies need to consider that BOLD signal changes also depend on baseline physiology, in particular OEF and venous blood volume (Archila-Melendez et al., 2021; Obata et al., 2004).

In addition, ICAS patients feature additional hemodynamic impairments, most importantly reductions in CVR and CBF, which could explain BOLD-FC reductions equally well. While our statistical analysis supports the view that the influence of CTH is stronger than the influence of baseline CBF, we cannot completely rule out that CVR might play an important role as well. This point certainly also needs further investigation based on high quality multi-parametric MRI data and more specific and detailed modelling.

5. Conclusion

Our empirical results demonstrate that increasing CTH differences between homotopic brain areas lead to BOLD-FC reductions, which can be well explained by our simulation results when considering increased CTH as an indicator of delayed and broadened CBF responses. Given these complex and non-linear influences as well as variable sources of vascular delays, i.e., macrovascular systemic as well as local microvascular contributions, we suggest that calibration approaches like linear regression of BOLD-TCs with vascular noise predictors (Liu et al., 2017; Erdoğan et al., 2016; Siegel et al., 2016; Christen et al., 2015) are not sufficient to fully recover information on underlying neuronal activity. We suggest to overcome the limitations of conventional rs-fMRI-based BOLD-FC analyses by combining our recent BOLD-FC simulation approach (Archila-Melendez et al., 2020) with comprehensive hemodynamic-oxygenation MRI, e.g., CVR, CBF, CBV, CTH and OEF, to aid the interpretation of BOLD-FC alterations in patient populations.

Funding

This work was supported by the German Research Foundation DFG [grant numbers PR 1039/6-1, SO 1336/4-1].

Data/code availability

The Matlab code of the simulation framework is publicly available at https://zenodo.org/record/3773316 and https://gitlab.lrz.de/nmrm_lab/public_projects/bold-simulation. This code was adapted for the systematic exploration of the dependence of BOLD-FC on CBF response timing. Dissemination of multi-parametric MRI data is restricted by ethics and privacy issues and therefore requires a formal data sharing agreement with the authors.

Ethical approval

The study was approved by the medical ethical board of the Klinikum rechts der Isar; for a detailed description of the overall sample characteristics see Table 1.

Informed consent

Participants provided written consent to all conducted examinations.

Declaration of competing interest

The authors declare that they have no conflict of interest.

Credit authorship contribution statement

Sebastian C. Schneider: Formal analysis, Investigation, Visualization, Writing – original draft, Writing – review & editing. **Mario E. Archila-Meléndez:** Conceptualization, Methodology, Software, Visualization, Writing – original draft, Writing – review & editing. **Jens Göttler:** Formal analysis, Investigation, Writing – review & editing. **Stephan Kaczmarz:** Formal analysis, Investigation, Writing – review & editing. **Benedikt Zott:** Writing – review & editing. **Josef Priller:** Writing – review & editing. **Michael Kallmayer:** Investigation, Writing – review & editing. **Claus Zimmer:** Resources, Writing – review & editing. **Christian Sorg:** Conceptualization, Supervision, Writing – original draft, Writing – review & editing. **Christine Preibisch:** Conceptualization, Methodology, Software, Visualization, Formal analysis, Investigation, Resources, Data curation, Supervision, Project administration, Funding acquisition, Writing – original draft, Writing – review & editing.

Acknowledgments

We thank Kim van de Ven (Philips Healthcare, Best, Netherlands) for her support with the ASL imaging and Kim Mouridsen and Mikkel Bo Hansen (both Center of Functionally Integrative Neuroscience, Aarhus University, Aarhus, Denmark) for their supplying software and support for CTH processing.

Supplementary materials

Supplementary material associated with this article can be found, in the online version, at doi:10.1016/j.neuroimage.2022.119208.

References

Aanerud, J., Borghammer, P., Rodell, A., Jónsdottir, K.Y., Gjedde, A., 2017. Sex differences of human cortical blood flow and energy metabolism. J. Cereb. Blood Flow Metab. 37 (7), 2433–2440.

Alisch, J.S.R., Khattar, N., Kim, R.W., Cortina, L.E., Rejimon, A.C., Qian, W., Ferrucci, L., Resnick, S.M., Spencer, R.G., Bouhrara, M., 2021. Sex and age-related differences in cerebral blood flow investigated using pseudo-continuous arterial spin labeling magnetic resonance imaging. Aging (Albany NY) 13 (4), 4911–4925.

Allen, E.A., Erhardt, E.B., Damaraju, E., Gruner, W., Segall, J.M., Silva, R.F., Havlicek, M., Rachakonda, S., Fries, J., Kalyanam, R., Michael, A.M., Caprihan, A., Turner, J.A., Eichele, T., Adelsheim, S., Bryan, A.D., Bustillo, J., Clark, V.P., Feldstein Ewing, S.W., Filbey, F., Ford, C.C., Hutchison, K., Jung, R.E., Kiehl, K.A., Kodituwakku, P., Komesu, Y.M., Mayer, A.R., Pearlson, G.D., Phillips, J.P., Sadek, J.R., Stevens, M., Teuscher, U., Thoma, R.J., Calhoun, V.D., 2011. A baseline for the multivariate comparison of resting-state networks. Front. Syst. Neurosci. 5, 2.

Alsop, D.C., Detre, J.A., Golay, X., Gunther, M., Hendrikse, J., Hernandez-Garcia, L., Lu, H., MacIntosh, B.J., Parkes, L.M., Smits, M., van Osch, M.J., Wang, D.J., Wong, E.C., Zaharchuk, G., 2015. Recommended implementation of arterial spin-labeled perfusion MRI for clinical applications: a consensus of the ISMRM perfusion study group and the European consortium for ASL in dementia. Magn. Reson. Med. 73, 102–116.

Amemiya, S., Kunimatsu, A., Saito, N., Ohtomo, K., 2012. Impaired hemodynamic response in the ischemic brain assessed with BOLD fMRI. Neuroimage 61, 579–590.

Ances, B.M., Liang, C.L., Leontiev, O., Perthen, J.E., Fleisher, A.S., Lansing, A.E., Buxton, R.B., 2009. Effects of aging on cerebral blood flow, oxygen metabolism, and blood oxygenation level dependent responses to visual stimulation. Hum. Brain Mapp. 30, 1120–1132.

Angleys, H., Jespersen, S.N., Østergaard, L., 2018. The effects of capillary transit time heterogeneity on the BOLD signal. Hum. Brain Mapp. 39 (6), 2329–2352.

Archila-Melendez, M.E., Sorg, C., Preibisch, C., 2020. Modeling the impact of neurovascular coupling impairments on BOLD-based functional connectivity at rest. Neuroimage 218, 116871.

Arsava, E.M., Hansen, M.B., Kaplan, B., Peker, A., Gocmen, R., Arat, A., Oguz, K.K., Topcuoglu, M.A., Østergaard, L., Dalkara, T., 2018. The effect of carotid artery stenting on capillary transit time heterogeneity in patients with carotid artery stenosis. Eur. Stroke J. 3, 263–271.

Avirame, K., Lesemann, A., List, J., Witte, A.V., Schreiber, S.J., Floel, A., 2015. Cerebral autoregulation and brain networks in occlusive processes of the internal carotid artery. J. Cereb. Blood Flow Metab. 35, 240–247.
Bates, D., Machler, M., Bolker, B.M., Walker, S.C., 2015. Fitting linear mixed-effects models using lme4. J. Stat. Softw. 67, 1–48.
Beall, E.B., Lowe, M.J., 2007. Isolating physiologic noise sources with independently determined spatial measures. Neuroimage 37 (4), 1286–1300.
Beall, E.B., Lowe, M.J., 2014. SimPACE: generating simulated motion corrupted BOLD data with synthetic-navigated acquisition for the development and evaluation of SLOMOCO: a new, highly effective slicewise motion correction. Neuroimage 101, 21–34.
Beishon, L., Clough, R.H., Kadicheeni, M., Chithiramohan, T., Panerai, R.B., Haunton, V.J., Minhas, J.S., Robinson, T.G., 2021. Vascular and haemodynamic issues of brain ageing. Pflugers Arch. 473, 735–751.
Blockley, N.P., Francis, S.T., Gowland, P.A., 2009. Perturbation of the BOLD response by a contrast agent and interpretation through a modified balloon model. Neuroimage 48, 84–93.
Brandl, F., Avram, M., Weise, B., Shang, J., Simoes, B., Bertram, T., Hoffmann Ayala, D., Penzel, N., Gursel, D.A., Bauml, J., Wohlschlager, A.M., Vukadinovic, Z., Koutsouleris, N., Leucht, S., Sorg, C., 2019. Specific substantial dysconnectivity in schizophrenia: a transdiagnostic multimodal meta-analysis of resting-state functional and structural magnetic resonance imaging studies. Biol. Psychiatry 85, 573–583.
Buckner, R.L., Krienen, F.M., Yeo, B.T., 2013. Opportunities and limitations of intrinsic functional connectivity MRI. Nat. Neurosci. 16, 832–837.
Buxton, R.B., Frank, L.R., Wong, E.C., Siewert, B., Warach, S., Edelman, R.R., 1998. A general kinetic model for quantitative perfusion imaging with arterial spin labeling. Magn. Reson. Med. 40, 383–396.
Buxton, R.B., Uludag, K., Dubowitz, D.J., Liu, T.T., 2004. Modeling the hemodynamic response to brain activation. Neuroimage 23 (1), S220–S233 Suppl.
Carnevale, L., Maffei, A., Landolfi, A., Grillea, G., Carnevale, D., Lembo, G., 2020. Brain functional magnetic resonance imaging highlights altered connections and functional networks in patients with hypertension. Hypertension 76 (5), 1480–1490.
Champagne, A.A., Coverdale, N.S., Ross, A., Chen, Y., Murray, C.I., Dubowitz, D., Cook, D.J., 2020. Multi-modal normalization of resting-state using local physiology reduces changes in functional connectivity patterns observed in mTBI patients. Neuroimage Clin. 26, 102204.
Chang, C., Leopold, D.A., Scholvinck, M.L., Mandelkow, H., Picchioni, D., Liu, X., Ye, F.Q., Turchi, J.N., Duyn, J.H., 2016a. Tracking brain arousal fluctuations with fMRI. Proc. Natl. Acad. Sci. USA 113, 4518–4523.
Chang, T.Y., Huang, K.L., Ho, M.Y., Ho, P.S., Chang, C.H., Liu, C.H., Chang, Y.J., Wong, H.F., Hsieh, I.C., Lee, T.H., Liu, H.L., 2016b. Graph theoretical analysis of functional networks and its relationship to cognitive decline in patients with carotid stenosis. J. Cereb. Blood Flow Metab. 36, 808–818.
Chao-Gan, Y., Yu-Feng, Z., 2010. DPARSF: a MATLAB toolbox for "Pipeline" data analysis of resting-state fMRI. Front. Syst. Neurosci. 4, 13.
Chen, Z., Zhang, X., Yuan, C., Zhao, X., van Osch, M.J.P., 2017. Measuring the labeling efficiency of pseudocontinuous arterial spin labeling. Magn. Reson. Med. 77, 1841–1852.
Cheng, H.L., Lin, C.J., Soong, B.W., Wang, P.N., Chang, F.C., Wu, Y.T., Chou, K.H., Lin, C.P., Tu, P.C., Lee, I.H., 2012. Impairments in cognitive function and brain connectivity in severe asymptomatic carotid stenosis. Stroke 43, 2567–2573.
Christen, T., Jahanian, H., Ni, W.W., Qiu, D., Moseley, M.E., Zaharchuk, G., 2015. Noncontrast mapping of arterial delay and functional connectivity using resting-state functional MRI: a study in Moyamoya patients. J. Magn. Reson. Imaging 41, 424–430.
Damaraju, E., Allen, E.A., Belger, A., Ford, J.M., McEwen, S., Mathalon, D.H., Mueller, B.A., Pearlson, G.D., Potkin, S.G., Preda, A., Turner, J.A., Vaidya, J.G., van Erp, T.G., Calhoun, V.D., 2014. Dynamic functional connectivity analysis reveals transient states of dysconnectivity in schizophrenia. Neuroimage Clin. 5, 298–308.
Daniel, D.G., Mathew, R.J., Wilson, W.H., 1989. Sex roles and regional cerebral blood flow. Psychiatry Res. 27 (1), 55–64.
De Vis, J.B., Bhogal, A.A., Hendrikse, J., Petersen, E.T., Siero, J.C.W., 2018. Effect sizes of BOLD CVR, resting-state signal fluctuations and time delay measures for the assessment of hemodynamic impairment in carotid occlusion patients. Neuroimage 179, 530–539.
De Vis, J.B., Hendrikse, J., Bhogal, A., Adams, A., Kappelle, L.J., Petersen, E.T., 2015. Age-related changes in brain hemodynamics; A calibrated MRI study. Hum. Brain Mapp. 36, 3973–3987.
D'Esposito, M., Deouell, L.Y., Gazzaley, A., 2003. Alterations in the BOLD fMRI signal with ageing and disease: a challenge for neuroimaging. Nat. Rev. Neurosci. 4, 863–872.
Drew, P.J., Mateo, C., Turner, K.L., Yu, X., Kleinfeld, D., 2020. Ultra-slow oscillations in fMRI and resting-state connectivity: neuronal and vascular contributions and technical confounds. Neuron 107, 782–804.
Duque, C., Feske, S.K., Sorond, F.A., 2017. Cerebrovascular hemodynamics in women. Semin. Neurol. 37 (6), 679–688.
Erdoğan, S.B., Tong, Y., Hocke, L.M., Lindsey, K.P., deB Frederick, B., 2016. Correcting for blood arrival time in global mean regression enhances functional connectivity analysis of resting state fMRI-BOLD signals. Front. Hum. Neurosci. 10, 311.
Farras-Permanyer, L., Mancho-Fora, N., Montala-Flaquer, M., Bartres-Faz, D., Vaque-Alcazar, L., Pero-Cebollero, M., Guardia-Olmos, J., 2019. Age-related changes in resting-state functional connectivity in older adults. Neural Regen. Res. 14, 1544–1555.
Feng, R., Rolls, E.T., Cheng, W., Feng, J., 2020. Hypertension is associated with reduced hippocampal connectivity and impaired memory. EBioMedicine 61, 103082.
Fox, M.D., Raichle, M.E., 2007. Spontaneous fluctuations in brain activity observed with functional magnetic resonance imaging. Nat. Rev. Neurosci. 8, 700–711.
Gottler, J., Kaczmarz, S., Kallmayer, M., Wustrow, I., Eckstein, H.H., Zimmer, C., Sorg, C., Preibisch, C., Hyder, F., 2019a. Flow-metabolism uncoupling in patients with asymptomatic unilateral carotid artery stenosis assessed by multi-modal magnetic resonance imaging. J. Cereb. Blood Flow Metab. 39, 2132–2143.
Gottler, J., Kaczmarz, S., Nuttall, R., Griese, V., Napiorkowski, N., Kallmayer, M., Wustrow, I., Eckstein, H.H., Zimmer, C., Preibisch, C., Finke, K., Sorg, C., 2020. The stronger one-sided relative hypoperfusion, the more pronounced ipsilateral spatial attentional bias in patients with asymptomatic carotid stenosis. J. Cereb. Blood Flow Metab. 40, 314–327.
Gottler, J., Preibisch, C., Riederer, I., Pasquini, L., Alexopoulos, P., Bohn, K.P., Yakushev, I., Beller, E., Kaczmarz, S., Zimmer, C., Grimmer, T., Drzezga, A., Sorg, C., 2019b. Reduced blood oxygenation level dependent connectivity is related to hypoperfusion in Alzheimer's disease. J. Cereb. Blood Flow Metab. 39, 1314–1325.
Gratton, C., Kraus, B.T., Greene, D.J., Gordon, E.M., Laumann, T.O., Nelson, S.M., Dosenbach, N.U.F., Petersen, S.E., 2020. Defining individual-specific functional neuroanatomy for precision psychiatry. Biol. Psychiatry 88, 28–39.
Hedderich, D., Kluge, A., Pyka, T., Zimmer, C., Kirschke, J.S., Wiestler, B., Preibisch, C., 2019. Consistency of normalized cerebral blood volume values in glioblastoma using different leakage correction algorithms on dynamic susceptibility contrast magnetic resonance imaging data without and with preload. J. Neuroradiol. 46, 44–51.
Jespersen, S.N., Ostergaard, L., 2012. The roles of cerebral blood flow, capillary transit time heterogeneity, and oxygen tension in brain oxygenation and metabolism. J. Cereb. Blood Flow Metab. 32, 264–277.
Joliot, M., Jobard, G., Naveau, M., Delcroix, N., Petit, L., Zago, L., Crivello, F., Mellet, E., Mazoyer, B., Tzourio-Mazoyer, N., 2015. AICHA: an atlas of intrinsic connectivity of homotopic areas. J. Neurosci. Methods 254, 46–59.
Kaczmarz, S., Göttler, J., Kooijman, H., van de Ven, K., Karampinos, D.C., Zimmer, C., Preibisch, C., 2016. Evaluation of pCASL sequences for CBF measures in healthy subjects and patients with high-grade carotid artery stenosis. In: 33rd Annual Scientific Meeting. ESMRMB (Ed.), Vienna, p. 204.
Kaczmarz, S., Gottler, J., Petr, J., Hansen, M.B., Mouridsen, K., Zimmer, C., Hyder, F., Preibisch, C., 2021. Hemodynamic impairments within individual watershed areas in asymptomatic carotid artery stenosis by multimodal MRI. J. Cereb. Blood Flow Metab. 41, 380–396.
Kaczmarz, S., Griese, V., Preibisch, C., Kallmayer, M., Helle, M., Wustrow, I., Petersen, E.T., Eckstein, H.H., Zimmer, C., Sorg, C., Gottler, J., 2018. Increased variability of watershed areas in patients with high-grade carotid stenosis. Neuroradiology 60, 311–323.
Kalisch, R., Elbel, G.K., Gössl, C., Czisch, M., Auer, D.P., 2001. Blood pressure changes induced by arterial blood withdrawal influence bold signal in anesthesized rats at 7 Tesla: implications for pharmacologic MRI. Neuroimage 14 (4), 891–898.
Kanda, T., Fukusato, T., Matsuda, M., Toyoda, K., Oba, H., Kotoku, J., Haruyama, T., Kitajima, K., Furui, S., 2015. Gadolinium-based contrast agent accumulates in the brain even in subjects without severe renal dysfunction: evaluation of autopsy brain specimens with inductively coupled plasma mass spectroscopy. Radiology 276, 228–232.
Katsel, P., Roussos, P., Pletnikov, M., Haroutunian, V., 2017. Microvascular anomaly conditions in psychiatric disease. Schizophrenia - angiogenesis connection. Neurosci. Biobehav. Rev. 77, 327–339.
Kleinfeld, D., Mitra, P.P., Helmchen, F., Denk, W., 1998. Fluctuations and stimulus-induced changes in blood flow observed in individual capillaries in layers 2 through 4 of rat neocortex. Proc. Natl. Acad. Sci. USA 95, 15741–15746.
Kluge, A., Lukas, M., Toth, V., Pyka, T., Zimmer, C., Preibisch, C., 2016. Analysis of three leakage-correction methods for DSC-based measurement of relative cerebral blood volume with respect to heterogeneity in human gliomas. Magn. Reson. Imaging 34, 410–421.
Kuznetsova, A., Brockhoff, P.B., Christensen, R.H.B., 2017. lmerTest Package: tests in linear mixed effects models. J. Stat. Softw. 82, 1–26.
Leenders, K.L., 1994. PET: blood flow and oxygen consumption in brain tumors. J. Neurooncol. 22, 269–273.
Lewis, N., Lu, H., Liu, P., Hou, X., Damaraju, E., Iraji, A., Calhoun, V., 2020. Static and dynamic functional connectivity analysis of cerebrovascular reactivity: an fMRI study. Brain Behav. 10, e01516.
Li, Z., Zhu, Y., Childress, A.R., Detre, J.A., Wang, Z., 2012. Relations between BOLD fMRI-derived resting brain activity and cerebral blood flow. PLoS One 7, e44556.
Liang, X., Zou, Q., He, Y., Yang, Y., 2013. Coupling of functional connectivity and regional cerebral blood flow reveals a physiological basis for network hubs of the human brain. Proc. Natl. Acad. Sci. USA 110, 1929–1934.
Lin, C.J., Tu, P.C., Chern, C.M., Hsiao, F.J., Chang, F.C., Cheng, H.L., Tang, C.W., Lee, Y.C., Chen, W.T., Lee, I.H., 2014. Connectivity features for identifying cognitive impairment in presymptomatic carotid stenosis. PLoS One 9, e85441.
Liu, T.T., Nalci, A., Falahpour, M., 2017. The global signal in fMRI: nuisance or Information? Neuroimage 150, 213–229.
Love, S., Miners, J.S., 2016. Cerebral hypoperfusion and the energy deficit in Alzheimer's disease. Brain Pathol. 26, 607–617.
Lv, Y., Margulies, D.S., Cameron Craddock, R., Long, X., Winter, B., Gierhake, D., Endres, M., Villringer, K., Fiebach, J., Villringer, A., 2013. Identifying the perfusion deficit in acute stroke with resting-state functional magnetic resonance imaging. Ann. Neurol. 73, 136–140.
Manoliu, A., Riedl, V., Zherdin, A., Muhlau, M., Schwerthoffer, D., Scherr, M., Peters, H., Zimmer, C., Forstl, H., Bauml, J., Wohlschlager, A.M., Sorg, C., 2014. Aberrant dependence of default mode/central executive network interactions on anterior insular salience network activity in schizophrenia. Schizophr. Bull. 40, 428–437.
Mark, C.I., Mazerolle, E.L., Chen, J.J., 2015. Metabolic and vascular origins of the BOLD effect: implications for imaging pathology and resting-state brain function. J. Magn. Reson. Imaging 42, 231–246.
Mateo, C., Knutsen, P.M., Tsai, P.S., Shih, A.Y., Kleinfeld, D., 2017. Entrainment of arteriole vasomotor fluctuations by neural activity is a basis of blood-oxygenation-level-dependent "resting-state" connectivity. Neuron 96 (4), 936–948 e3.

Mouridsen, K., Friston, K., Hjort, N., Gyldensted, L., Østergaard, L., Kiebel, S., 2006. Bayesian estimation of cerebral perfusion using a physiological model of microvasculature. Neuroimage 33 (2), 570–579.
Mouridsen, K., Hansen, M.B., Ostergaard, L., Jespersen, S.N., 2014. Reliable estimation of capillary transit time distributions using DSC-MRI. J. Cereb. Blood Flow Metab. 34, 1511–1521.
Mundiyanapurath, S., Ringleb, P.A., Diatschuk, S., Hansen, M.B., Mouridsen, K., Ostergaard, L., Wick, W., Bendszus, M., Radbruch, A., 2016. Capillary transit time heterogeneity is associated with modified Rankin scale score at discharge in patients with bilateral high grade internal carotid artery stenosis. PLoS One 11, e0158148.
Murphy, K., Fox, M.D., 2017. Towards a consensus regarding global signal regression for resting state functional connectivity MRI. Neuroimage 154, 169–173.
NASCET, 1991. North American symptomatic carotid endarterectomy trial. Methods, patient characteristics, and progress. Stroke 22, 711–720.
Nielsen, R.B., Parbo, P., Ismail, R., Dalby, R., Tietze, A., Braendgaard, H., Gottrup, H., Brooks, D.J., Ostergaard, L., Eskildsen, S.F., 2020. Impaired perfusion and capillary dysfunction in prodromal Alzheimer's disease. Alzheimers Dement. (Amst) 12, e12032.
Nuttall, R., Pasquini, L., Scherr, M., Sorg, C., 2016. Degradation in intrinsic connectivity networks across the Alzheimer's disease spectrum. Alzheimers Dement. (Amst) 5, 35–42.
Obata, T., Liu, T.T., Miller, K.L., Luh, W.M., Wong, E.C., Frank, L.R., Buxton, R.B., 2004. Discrepancies between BOLD and flow dynamics in primary and supplementary motor areas: application of the balloon model to the interpretation of BOLD transients. Neuroimage 21, 144–153.
Ostergaard, L., Aamand, R., Gutierrez-Jimenez, E., Ho, Y.C., Blicher, J.U., Madsen, S.M., Nagenthiraja, K., Dalby, R.B., Drasbek, K.R., Moller, A., Braendgaard, H., Mouridsen, K., Jespersen, S.N., Jensen, M.S., West, M.J., 2013a. The capillary dysfunction hypothesis of Alzheimer's disease. Neurobiol. Aging 34, 1018–1031.
Ostergaard, L., Chesler, D.A., Weisskoff, R.M., Sorensen, A.G., Rosen, B.R., 1999. Modeling cerebral blood flow and flow heterogeneity from magnetic resonance residue data. J. Cereb. Blood Flow Metab. 19 (6), 690–699.
Ostergaard, L., Engedal, T.S., Moreton, F., Hansen, M.B., Wardlaw, J.M., Dalkara, T., Markus, H.S., Muir, K.W., 2016. Cerebral small vessel disease: capillary pathways to stroke and cognitive decline. J. Cereb. Blood Flow Metab. 36, 302–325.
Ostergaard, L., Jespersen, S.N., Mouridsen, K., Mikkelsen, I.K., Jonsdottir, K.Y., Tietze, A., Blicher, J.U., Aamand, R., Hjort, N., Iversen, N.K., Cai, C., Hougaard, K.D., Simonsen, C.Z., Von Weitzel-Mudersbach, P., Modrau, B., Nagenthiraja, K., Riisgaard Ribe, L., Hansen, M.B., Bekke, S.L., Dahlman, M.G., Puig, J., Pedraza, S., Serena, J., Cho, T.H., Siemonsen, S., Thomalla, G., Fiehler, J., Nighoghossian, N., Andersen, G., 2013b. The role of the cerebral capillaries in acute ischemic stroke: the extended penumbra model. J. Cereb. Blood Flow Metab. 33, 635–648.
Ostergaard, L., Weisskoff, R.M., Chesler, D.A., Gyldensted, C., Rosen, B.R., 1996. High resolution measurement of cerebral blood flow using intravascular tracer bolus passages. Part I: mathematical approach and statistical analysis. Magn. Reson. Med. 36 (5), 715–725.
Potreck, A., Loebel, S., Pfaff, J., Ostergaard, L., Mouridsen, K., Radbruch, A., Bendszus, M., Mundiyanapurath, S., 2019. Increased volumes of mildly elevated capillary transit time heterogeneity positively predict favorable outcome and negatively predict intracranial hemorrhage in acute ischemic stroke with large vessel occlusion. Eur. Radiol. 29, 3523–3532.
Power, J.D., Barnes, K.A., Snyder, A.Z., Schlaggar, B.L., Petersen, S.E., 2012. Spurious but systematic correlations in functional connectivity MRI networks arise from subject motion. Neuroimage 59, 2142–2154.
Powers, W.J., Fox, P.T., Raichle, M.E., 1988. The effect of carotid artery disease on the cerebrovascular response to physiologic stimulation. Neurology 38, 1475–1478.
Powers, W.J., Press, G.A., Grubb Jr., R.L., Gado, M., Raichle, M.E., 1987. The effect of hemodynamically significant carotid artery disease on the hemodynamic status of the cerebral circulation. Ann. Intern. Med. 106, 27–34.
Preibisch, C., Sorg, C., Forschler, A., Grimmer, T., Sax, I., Wohlschlager, A.M., Perneczky, R., Forstl, H., Kurz, A., Zimmer, C., Alexopoulos, P., 2011. Age-related cerebral perfusion changes in the parietal and temporal lobes measured by pulsed arterial spin labeling. J. Magn. Reson. Imaging 34, 1295–1302.
Qiu, M., Scheinost, D., Ramani, R., Constable, R.T., 2017. Multi-modal analysis of functional connectivity and cerebral blood flow reveals shared and unique effects of propofol in large-scale brain networks. Neuroimage 148, 130–140.
Rasmussen, P.M., Jespersen, S.N., Østergaard, L., 2015. The effects of transit time heterogeneity on brain oxygenation during rest and functional activation. Cerebr. Blood Flow Metab. 35, 432–442.
RCoreTeam, 2020. R: A Language and Environment for Statistical Computing. Computing, R.F.f.S. (Ed.).
Reimann, H.M., Todiras, M., Hodge, R., Huelnhagen, T., Millward, J.M., Turner, R., Seeliger, E., Bader, M., Pohlmann, A., Niendorf, T., 2018. Somatosensory BOLD fMRI reveals close link between salient blood pressure changes and the murine neuromatrix. Neuroimage 172, 562–574.
Richter, V., Helle, M., van Osch, M.J., Lindner, T., Gersing, A.S., Tsantilas, P., Eckstein, H.H., Preibisch, C., Zimmer, C., 2017. MR imaging of individual perfusion reorganization using superselective pseudocontinuous arterial spin-labeling in patients with complex extracranial steno-occlusive disease. AJNR Am. J. Neuroradiol. 38, 703–711.
Riederer, I., Bohn, K.P., Preibisch, C., Wiedemann, E., Zimmer, C., Alexopoulos, P., Forster, S., 2018. Alzheimer disease and mild cognitive impairment: integrated pulsed arterial spin-labeling MRI and (18)F-FDG PET. Radiology 288, 198–206.
RStudioTeam, 2019. RStudio: Integrated Development Environment for R. RStudio, I. (Ed.).
Scholvinck, M.L., Maier, A., Ye, F.Q., Duyn, J.H., Leopold, D.A., 2010. Neural basis of global resting-state fMRI activity. Proc. Natl. Acad. Sci. USA 107, 10238–10243.
Schroeder, T., 1988. Hemodynamic significance of internal carotid artery disease. Acta Neurol. Scand. 77, 353–372.
Schulte, M.L., Wood, J.D., Hudetz, A.G., 2003. Cortical electrical stimulation alters erythrocyte perfusion pattern in the cerebral capillary network of the rat. Brain Res. 963, 81–92.
Siegel, J.S., Power, J.D., Dubis, J.W., Vogel, A.C., Church, J.A., Schlaggar, B.L., Petersen, S.E., 2014. Statistical improvements in functional magnetic resonance imaging analyses produced by censoring high-motion data points. Hum. Brain Mapp. 35, 1981–1996.
Siegel, J.S., Snyder, A.Z., Ramsey, L., Shulman, G.L., Corbetta, M., 2016. The effects of hemodynamic lag on functional connectivity and behavior after stroke. J. Cereb. Blood Flow Metab. 36, 2162–2176.
Siero, J.C., Hartkamp, N.S., Donahue, M.J., Harteveld, A.A., Compter, A., Petersen, E.T., Hendrikse, J., 2015. Neuronal activation induced BOLD and CBF responses upon acetazolamide administration in patients with steno-occlusive artery disease. Neuroimage 105, 276–285.
Simon, A.B., Buxton, R.B., 2015. Understanding the dynamic relationship between cerebral blood flow and the BOLD signal: implications for quantitative functional MRI. Neuroimage 116, 158–167.
Son, S.J., Kim, J., Lee, E., Park, J.Y., Namkoong, K., Hong, C.H., Ku, J., Kim, E., Oh, B.H., 2015. Effect of hypertension on the resting-state functional connectivity in patients with Alzheimer's disease (AD). Arch. Gerontol. Geriatr. 60 (1), 210–216.
Stefanovic, B., Hutchinson, E., Yakovleva, V., Schram, V., Russell, J.T., Belluscio, L., Koretsky, A.P., Silva, A.C., 2008. Functional reactivity of cerebral capillaries. J. Cereb. Blood Flow Metab. 28, 961–972.
Tong, Y., Lindsey, K.P., Hocke, L.M., Vitaliano, G., Mintzopoulos, D., Frederick, B.D., 2017. Perfusion information extracted from resting state functional magnetic resonance imaging. J. Cereb. Blood Flow Metab. 37, 564–576.
Tong, Y., Yao, J.F., Chen, J.J., Frederick, B.D., 2019. The resting-state fMRI arterial signal predicts differential blood transit time through the brain. J. Cereb. Blood Flow Metab. 39, 1148–1160.
Tsvetanov, K.A., Henson, R.N., Tyler, L.K., Razi, A., Geerligs, L., Ham, T.E., Rowe, J.B., 2016. Extrinsic and intrinsic brain network connectivity maintains cognition across the lifespan despite accelerated decay of regional brain activation. J. Neurosci. 36, 3115–3126.
Tsvetanov, K.A., Henson, R.N.A., Rowe, J.B., 2021. Separating vascular and neuronal effects of age on fMRI BOLD signals. Philos. Trans. R. Soc. Lond. B Biol. Sci. 376, 20190631.
Turchi, J., Chang, C., Ye, F.Q., Russ, B.E., Yu, D.K., Cortes, C.R., Monosov, I.E., Duyn, J.H., Leopold, D.A., 2018. The basal forebrain regulates global resting-state fMRI fluctuations. Neuron 97, 940–952 e944.
van Niftrik, C.H.B., Piccirelli, M., Muscas, G., Sebok, M., Fisher, J.A., Bozinov, O., Stippich, C., Valavanis, A., Regli, L., Fierstra, J., 2019. The voxel-wise analysis of false negative fMRI activation in regions of provoked impaired cerebrovascular reactivity. PLoS One 14, e0215294.
Varangis, E., Habeck, C.G., Razlighi, Q.R., Stern, Y., 2019. The effect of aging on resting state connectivity of predefined networks in the brain. Front. Aging Neurosci. 11, 234.
Wang, T., Xiao, F., Wu, G., Fang, J., Sun, Z., Feng, H., Zhang, J., Xu, H., 2017. Impairments in brain perfusion, metabolites, functional connectivity, and cognition in severe asymptomatic carotid stenosis patients: an integrated MRI study. Neural Plast. 2017, 8738714.
West, K.L., Zuppichini, M.D., Turner, M.P., Sivakolundu, D.K., Zhao, Y., Abdelkarim, D., Spence, J.S., Rypma, B., 2019. BOLD hemodynamic response function changes significantly with healthy aging. Neuroimage 188, 198–207.
Winder, A.T., Echagarruga, C., Zhang, Q., Drew, P.J., 2017. Weak correlations between hemodynamic signals and ongoing neural activity during the resting state. Nat. Neurosci. 20 (12), 1761–1769.
Yeo, B.T., Krienen, F.M., Sepulcre, J., Sabuncu, M.R., Lashkari, D., Hollinshead, M., Roffman, J.L., Smoller, J.W., Zollei, L., Polimeni, J.R., Fischl, B., Liu, H., Buckner, R.L., 2011. The organization of the human cerebral cortex estimated by intrinsic functional connectivity. J. Neurophysiol. 106, 1125–1165.
Yoshikawa, A., Masaoka, Y., Yoshida, M., Koiwa, N., Honma, M., Watanabe, K., Kubota, S., Natsuko, I., Ida, M., Izumizaki, M., 2020. Heart rate and respiration affect the functional connectivity of default mode network in resting-state functional magnetic resonance imaging. Front. Neurosci. 14, 631.
Zhou, J., Greicius, M.D., Gennatas, E.D., Growdon, M.E., Jang, J.Y., Rabinovici, G.D., Kramer, J.H., Weiner, M., Miller, B.L., Seeley, W.W., 2010. Divergent network connectivity changes in behavioural variant frontotemporal dementia and Alzheimer's disease. Brain 133, 1352–1367.
Zhou, J., Seeley, W.W., 2014. Network dysfunction in Alzheimer's disease and frontotemporal dementia: implications for psychiatry. Biol. Psychiatry 75, 565–573.